

# Sensitivity of tropospheric loads and lifetimes of short lived pollutants to fire emissions

N. Daskalakis<sup>1,2</sup>, S. Myriokefalitakis<sup>1</sup>, and M. Kanakidou<sup>1</sup>

[1]((Environmental Chemical Processes Laboratory, Department of Chemistry, University of Crete, Heraklion, Crete, Greece))

[2]((Institute of Chemical Engineering Sciences (ICE-HT), FORTH, Patra, Greece))

Correspondence to: M. Kanakidou (mariak@chemistry.uoc.gr)

## Abstract

The capability of global Chemistry and Transport Models (CTMs) to simulate atmospheric composition and its spatial and temporal changes highly relies on the input data used by the models, in particular the emission inventories. Biomass burning emissions show large spatial, diurnal, seasonal and year-to-year variability. In the present study, we applied a global 3D CTM to evaluate uncertainties in the computed atmospheric composition associated with the use of different biomass burning emissions and identify areas where observational data can help to reduce these uncertainties. We find the emission inventory choice to lead to regional differences in the calculated load of aerosols up to a factor of 4. Assumptions on the injection height of the biomass burning emissions are found to produce regionally up to 30% differences in the calculated tropospheric lifetimes of pollutants. Computed changes in lifetimes point to a strong chemical feedback mechanism between emissions from biomass burning and isoprene emissions from vegetation that are linked via NO<sub>x</sub>-driven oxidant chemistry, NO<sub>x</sub>-dependent changes in isoprene oxidation products, aerosol emissions and atmospheric transport. These interactions reduce isoprene load in the presence of biomass burning emissions by 15%, calculated for the same amount of isoprene emitted into the troposphere. Thus, isoprene load and lifetime are inversely related to the quantities of pollutants emitted by biomass burning. This feedback is shown to be able to increase the global annual secondary aerosol yield from isoprene emissions, defined as the ratio of tropospheric loads of secondary aerosol from isoprene oxidation to isoprene emissions, by up to 18%.

# 1 **1 Introduction**

2 Atmospheric composition is affected by emissions of reactive gases and aerosols to the  
3 atmosphere by several natural (e.g. soils, vegetation, oceans, volcanoes, wild fires) and  
4 anthropogenic sources (e.g. industrial and residential activities, transport, and shipping).  
5 Among these sources biomass burning plays a central role for atmospheric chemistry via  
6 changes in the atmospheric composition but also impacting on the ecosystem functioning  
7 through atmospheric deposition of nutrients and the lifecycle of vegetation (Keywood et al.,  
8 2013). Biomass burning is positioned between the natural (wild fires) and human-induced  
9 (intentional burning) sources of atmospheric pollutants since a fraction of open fires is  
10 induced by humans for agricultural and city expansion purposes (Levine et al., 1995) or for  
11 protection against fire itself (Mutch, 1994). Biomass burning is an important source of trace  
12 constituents to the atmosphere including radiatively and chemically reactive gases and  
13 aerosols (Andreae and Merlet, 2001; Akagi et al., 2011). It is the largest source of primary  
14 carbonaceous aerosols (Bond et al., 2004) and the second largest source of volatile organic  
15 compounds (VOC) in the atmosphere after the emissions from vegetation (Guenther et al.,  
16 2012) and of carbon monoxide (CO) after anthropogenic emissions (Kanakidou and Crutzen,  
17 1999; Pfister et al., 2005).

18 Emissions from biomass burning and their transformation in the atmosphere affect air quality  
19 (Lelieveld et al., 2004), interact with radiation (Reid et al., 2005) and the atmospheric water  
20 cycle and thus affect climate (Rosenfeld, 1999). In turn climate change is seen to impact on  
21 wild fire occurrence and intensity. For instance the exceptionally intensive 1997/1998  
22 Indonesia fires have been attributed to the combined strength of the El Niño and the Indian  
23 Ocean Dipole (Field et al., 2009).

24 Significant changes in the trends of atmospheric concentrations of CH<sub>4</sub> and CO have been  
25 attributed to the changes in the biomass burning emissions (Simmonds et al., 2005). Most of  
26 these emissions occur in the tropics that are subject to intensive photochemistry in the  
27 presence of high humidity conditions and significant convective activities (Chatfield and  
28 Delany, 1990; Crutzen, 1994). During summer in the high latitudes boreal forest fires  
29 contribute about 12% to the global biomass burning emissions (Lavoué et al., 2000) and can  
30 be so intensive and convective that their emissions reach the high troposphere and low  
31 stratosphere (Fromm et al., 2000).

1 Tropical photochemistry is controlling the lifetime of most atmospheric pollutants (Crutzen,  
2 1994; Keywood et al., 2013), including reactive greenhouse gases like methane (CH<sub>4</sub>) and  
3 ozone (O<sub>3</sub>), and thus their persistence in the atmosphere to impact on radiation and climate.  
4 Up to about 25% of the net global photochemical production of tropospheric ozone has been  
5 attributed to biomass burning emissions and chemistry in the atmosphere (Crutzen and  
6 Andreae, 1990; Jaffe and Wigder, 2012). Long range transport of biomass burning aerosols  
7 has been seen to happen fast within one or two weeks both downwind tropical (Edwards et al.,  
8 2006; Dirksen et al., 2009) and high latitude sources (Jaffe et al., 2004). Thus this source is  
9 affecting atmospheric pollutant levels in remote environments. For instance, chemical ageing  
10 of fire plumes has been identified as contributor to the high ozone over the Atlantic ocean  
11 (Lelieveld et al., 2004). Therefore it is important to simulate the impact of biomass burning  
12 emissions on tropospheric composition and pollutant lifetimes and to evaluate the  
13 uncertainties in such simulations.

14 Several biomass burning emission inventories have been constructed based on burned area,  
15 active fire detections, and plant productivity from satellite observations (van der Werf et al.,  
16 2010) or on assimilated Fire Radiative Power derived from satellite observations (Kaiser et  
17 al., 2012) and experimentally determined pollutant emission factors (Andreae and Merlet,  
18 2001) and assumptions on the state of burning of the biomass (smoldering or flaming, van der  
19 Werf et al. (2006)). All these factors introduce uncertainties in the emissions (Granier et al.,  
20 2011; Wiedinmyer et al., 2011). In particular, the size of small fires can be overestimated and  
21 the number of fires can be underestimated when seen by satellites (Wiedinmyer et al., 2011).  
22 The injection height of fire emissions (Dentener et al., 2006; Freitas et al., 2007; Sofiev et al.,  
23 2012) is an additional cause of discrepancies in the model estimates of the impact of these  
24 fires on tropospheric composition. The height distribution proposed by Dentener et al. (2006)  
25 (used in this work) is based on wildfire location and type, where the distribution described in  
26 Sofiev et al. (2012) is based on the fire characteristics (fire intensity, temperature of plume,  
27 type of source) as well as the meteorological conditions (atmospheric boundary layer height,  
28 free troposphere). These two approaches show similarities in emission heights over North  
29 America and Oceania, but over Eurasia, Australia and South America the two methods show  
30 significant differences (Sofiev et al., 2013). A plume height climatology over North America  
31 has been also derived by analysis of 5-year satellite observations by MISR (Val Martin et al.,  
32 2010) which compared to the Dentener et al (2006) vertical distribution of fires there (2000-

1 6000 meters) shows lower mean injection heights (500-1500 meters) for boreal fires but is in  
2 agreement for temperate and tropical fires. Plume rise models evaluated against that  
3 climatology have been shown to underestimate the observed plume heights (Val Martin et al.,  
4 2012). Guan et al. (2008) using the NCAR CAM3.1 model found that the calculated CO  
5 concentrations downwind biomass burning emission areas, can increase by up to 150 ppb  
6 depending on the assumptions in the injection height of the emissions. Boreal forest fire  
7 emissions occurring high in the troposphere have been detected by Colarco et al. (2004) to be  
8 transported from Canada to Washington D.C. in the U.S.A. where they have been mixed with  
9 boundary layer air. Long range transport of biomass burning pollutants has been followed by  
10 lidar and satellite observations and the simulations have been shown to be sensitive to the  
11 injection height of the emissions as well as to the entrainment of air into the boundary layer  
12 over U.S.A. Note that boreal fires plumes can reach the upper troposphere where their impact  
13 is different from that in the boundary layer due to the non-linearities in the atmospheric  
14 chemistry (Chatfield and Delany, 1990) and the different photochemical conditions there.  
15 Leung et al. (2007) global modeling study of the impact of boreal fire emissions on air  
16 pollutants levels, found a much larger enhancement in ozone when about half the emissions  
17 were released above the boundary layer than when all emissions were occurring in the  
18 boundary layer. They attributed these differences to the role of peroxyacetyl nitrate (PAN) as  
19 carrier of NO<sub>x</sub> downwind burning areas. Jaffe et al. (2004) found that the intensive Siberian  
20 fires in 2003 enhanced the background ozone over the Pacific Northwest U.S.A., resulting to  
21 exceedance of ozone air quality standard. Hodzic et al. (2006) studying AOT over Europe  
22 during the 2003 Portuguese fires identified high altitude transport of smoke particles from  
23 Portugal to The Netherlands, that has been both observed by POLDER-2 and simulated by the  
24 CHIMERE model. Williams et al. (2012) simulated the African fires in 2005 using the TM4  
25 model and three different biomass burning emission inventories, two global and one regional.  
26 They calculated differences in the ozone global burden resulting from the use of different  
27 biomass burning inventories that range between +1.7% and +4.6% compared to the simulation  
28 using GFEDv3 biomass burning emission inventory.

29 The present study aims to evaluate uncertainties in model estimates of biomass burning  
30 impacts on atmospheric composition that are associated with the use of different emission  
31 inventories in the same model. The study also aims to identify locations where additional  
32 observations can provide constrains for biomass burning emission estimates. For this purpose

1 a global 3D Chemistry and Transport Model (CTM) is applied to evaluate uncertainties in the  
2 atmospheric composition and major pollutants lifetimes computed using recently updated and  
3 commonly used biomass burning emissions. Based on the computed model sensitivity to  
4 biomass burning emissions, we also identify areas where observational data can help to  
5 reduce these uncertainties.

6

## 7 **2 Model Description**

8 The model used for this study is the global 3-D CTM TM4-ECPL (Kanakidou et al., 2012).  
9 The model accounts for gas and multiphase chemistry to describe tropospheric ozone  
10 chemistry and all major aerosol components (primary and secondary). It contains explicit  
11 chemistry of C<sub>1</sub> to C<sub>5</sub> volatile organic compounds (VOCs) and a highly simplified  
12 representation of *α*-pinene and *β*-pinene chemistry. The model calculates secondary organic  
13 aerosol (SOA) formation by VOC oxidation and subsequent gas-to-particle partitioning of  
14 semivolatile products (Tsigaridis and Kanakidou (2007) as updated by Myriokefalitakis et al.  
15 (2010)). Chemical aging of organic aerosol (OA) is also taken into account. For primary  
16 organic aerosol (POA) and black carbon (BC) chemical ageing is considered to occur by  
17 oxidation of organic material that coats the particles and is driven by O<sub>3</sub> (Tsigaridis and  
18 Kanakidou, 2003); while for SOA chemical ageing to non-volatile SOA (Tsigaridis and  
19 Kanakidou, 2003) is considered to occur by reaction with OH at the rate of  $4 \cdot 10^{-12} \text{ molec}^{-1}$   
20  $\text{cm}^3 \text{s}^{-1}$ , very close to that of the H-abstraction reaction of pinonic acid with OH (Praplan et  
21 al., 2012). BC emissions are by 20% soluble while terrestrial POA emissions are by 50%  
22 soluble. For both BC and POA the insoluble fraction is converted to soluble during aging.  
23 Multiphase chemical production of SOA is parameterized as described in Myriokefalitakis et  
24 al. (2011). Gas-to-particle partitioning of inorganic components is solved using the  
25 ISORROPIA II aerosol thermodynamic model that also calculates the aerosol-water (Nenes et  
26 al., 1998; Fountoukis and Nenes, 2007). For this study the TM4-ECPL model uses a 3°x2°  
27 longitude-latitude grid and 34 hybrid levels up to 0.1 hPa (with the first 4 model vertical  
28 layers between surface and 900 hPa) and is driven by the European Centre for Medium-range  
29 Weather Forecasts (ECMWF) ERA-Interim meteorological data (Dee et al., 2011) for the year  
30 2008 for all the sensitivity simulations.

## 1 **2.1 Natural emissions**

2 Isoprene, terpenes and biogenic volatile organic compounds (BVOC) emissions in the TM4-  
3 ECPL model are taken from the MEGAN-MACC inventory (Sindelarova et al., 2014) for the  
4 year 2008, which is a product of the MEGANv2.1 model (Guenther et al., 2012). Dust  
5 emissions are from AeroCom (Aerosol Comparisons between Observations and Models;  
6 (Dentener et al., 2006) calculated for the year 2008 by E. Vignati (personal communication,  
7 2011). Marine emissions of sea-salt aerosols and organic gases and aerosols are calculated  
8 online driven by meteorology and sea water productivity as described by Myriokefalitakis et  
9 al. (2010) and Vignati et al. (2010).

## 10 **2.2 Anthropogenic emissions**

11 Anthropogenic emissions used for this experiment are the ECLIPSE (Evaluating the CLimate  
12 and Air Quality ImPacts of Short-livEd Pollutants) version 4.0 emissions (Klimont et al.,  
13 2013), available in  $0.5^\circ \times 0.5^\circ$  spatial resolution. The ECLIPSE anthropogenic inventory was  
14 initially provided as sectoral including the agricultural waste burning sector (AWB). Since  
15 AWB is either included in the anthropogenic emissions or in the biomass burning emissions,  
16 caution was taken to avoid double counting of the emissions. For this, the AWB emissions  
17 (Table 3) are considered separately for the simulations that have been performed for this study  
18 (Table 4). The AWB in the ECLIPSE database amounts to 4.5% of the total anthropogenic  
19 pollutants emissions (approximately  $34.5 \text{ Tg a}^{-1}$ ) for the year 2008 (see Table 1 for more  
20 information). Anthropogenic emissions of all basic pollutants are used (CO, nitrogen oxides  
21 ( $\text{NO}_x$ ), black carbon aerosol (BC), particulate organic carbon (OC), sulfur dioxide and sulfates  
22 ( $\text{SO}_x$ ) as well as speciated non methane volatile organic compounds (NMVOCs; for a list of  
23 the NMVOCs used in the model see supplementary material S1).

## 24 **2.3 Biomass burning emissions**

25 For the present study a number of sensitivity simulations have been performed (Table 4) using  
26 different biomass burning emissions (Table 2) and AWB emissions (Table 3), all for the year  
27 2008. For the base simulation (S0.0), the biomass burning emissions from the Global Fire  
28 Emission Database v 3.1 (GFEDv3; van der Werf et al. (2010)) are used, excluding the AWB  
29 sector (Table 3), hereafter called GFEDv3-ECLIPSE biomass burning emissions (S0.X),  
30 while AWB emissions are taken from the ECLIPSE anthropogenic emissions developed in the

1 framework of the ECLIPSE project. Additional simulations have been performed (Table 4)  
2 using both biomass burning and AWB emissions from the GFEDv3 (van der Werf et al.,  
3 2010) (S1.X), as well as AWB from ECLIPSE and biomass burning emissions from the  
4 Atmospheric Chemistry and Climate Model Intercomparison Project's (ACCMIP; Lamarque  
5 et al. (2013); <http://ecaad.sedoo.fr>) (S2.X) or from the Fire INventory from NCAR (FINN;  
6 Wiedinmyer et al. (2011) <http://bai.acd.ucar.edu/Data/fire/>) (S3.X) and finally a simulation  
7 where no biomass burning emissions were taken into account (S4.0). Since the injection  
8 height of these emissions contributes to the uncertainty of the model results, biomass burning  
9 emissions are considered in the model either to be injected at heights following Dentener et al.  
10 (2006), or to be emitted solely in the lowest model layer (see list of simulations in Table 4).  
11 The temporal variability of these biomass burning inventories per emitted species for 2008 is  
12 shown in Fig. 1. This figure depicts the differences between the inventories in their  
13 seasonality and amplitude (also annual totals in Table 2); while Fig S2 in the supplementary  
14 material shows spatial difference in the annual BC emissions between the inventories. The  
15 ACCMIP inventory shows the largest magnitude in the temporal variation of these emissions.  
16 All inventories show a July-Sept. primary maximum while they differ in the secondary  
17 maximum between Jan and April. The AWB emissions that are not included in the GFEDv3-  
18 ECLIPSE biomass burning inventory significantly contribute to NMVOC and NH<sub>3</sub> emissions  
19 during spring and summer.

### 20 **3 Experiment setup**

21 The impact of the use of different biomass burning emission inventories to the calculated  
22 tropospheric loads and lifetimes of the main pollutants and the sensitivity of the model results  
23 to the wild fire emissions have been evaluated based on nine different simulations. For all  
24 simulations the model setup was exactly the same, except for the biomass burning emissions  
25 inventory used and its vertical distribution application. A summary of the simulations here  
26 performed is provided in Table 4. The GFEDv3-ECLIPSE inventory and height distribution  
27 for biomass burning emissions have been used as the base case scenario (S0.0). All scenarios  
28 named SX.0 assume the same fractional height distribution of the emissions according to  
29 Dentener et al. (2006) where all the scenarios named SX.1 assume all open biomass burning  
30 emissions to occur at surface. For scenario S4.0, open biomass burning emissions are set to  
31 zero. Note that we have chosen to account for monthly mean emissions since not all

1 inventories have higher temporal resolution. This is the reason we have also chosen to  
2 validate the model results comparing to monthly mean observations.

### 3 **4 Results**

4 To evaluate the ability of the model to reproduce the observations, the computed  
5 concentrations are compared with measurements. The differences in the fields computed by  
6 the various emission inventories provide a measure for the robustness of the model results  
7 with regard to the biomass burning impacts. Comparison of the simulated tropospheric  
8 concentrations of pollutants between the various scenarios reveals the spatial and temporal  
9 differences due to the different inventories and could indicate which inventory is performing  
10 the best. Ultimately these differences will point to areas where additional observations can  
11 contribute to reduce uncertainties of the emission inventories as will be further discussed.  
12 Finally, tropospheric lifetimes are calculated to provide information on how the location and  
13 strength of the emissions affect the persistence of the pollutants in the atmosphere.

#### 14 **4.1 Comparison with ground measurements**

15 Surface observations of Ozone from the European Monitoring and Evaluation Programme  
16 (EMEP) monitoring network (Europe), Ozone and CO observations from the World Data  
17 Centre for Greenhouse Gases (WDCGG) database (Global) and particulate Organic Carbon  
18 (OC) observations from the Aerosol Comparisons between Observations and Models  
19 (AeroCom) phase II database (Global) (Tsigaridis et al., 2014) have been used for the model  
20 evaluation. The locations of measurements are shown in Fig. S1 in the supplement. While all  
21 available data have been used for model evaluation, only comparisons at stations that have  
22 been selected to make evident differences between the simulations using different biomass  
23 burning emission inventories are shown for OC (Fig. 2), CO (Fig. 3) and O<sub>3</sub> (Fig. 4).  
24 Concentration fields of primary pollutants emitted by biomass burning are more strongly  
25 affected by the different emission inventories and injection heights. Thus, OC computed  
26 concentrations (Fig. 2) and BC concentrations (not shown) present the largest diversity,  
27 between simulations followed by CO (Fig. 3), which is emitted by fires, but has also  
28 secondary sources.

29 The simulated OC for the various scenarios and their differences from the observations in the  
30 tropics, the subtropics and high latitudes at locations affected by biomass burning emissions



1 are shown in Fig. 2. Due to limited observational data from the tropics where most of the  
2 biomass burning occurs, for the following comparisons all available data have been used  
3 independent of the year. Modeled differences for OC due to emission inventory choice can  
4 exceed a factor of three at Alta Floresta (Fig. 2c) and eight at Rondonia (Fig. 2d) during the  
5 biomass burning months. Using the ACCMIP inventory the largest OC levels are computed at  
6 the tropical station of Alta Floresta in August and September, whereas the GFEDv3-ECLIPSE  
7 and GFEDv3 inventories include large amounts of OC injections at the subtropical stations of  
8 California in June, July and August (Fig. 2b and g). Different emission inventories  
9 significantly affect the model performance over and downwind locations where wildfires  
10 occur. Unfortunately, current observational sites do not provide sufficient constraint for the  
11 emission databases evaluation.

12 Tsigaridis et al. (2014) OC global model intercomparison exercise has indicated that among  
13 the thirty-one models contributing to that study, some models emit all biomass burning  
14 aerosols at the surface, while most models distribute them to a number of layers above the  
15 surface, typically within the boundary layer. Most models are using GFEDv3 and ACCMIP  
16 inventories and all models appear to have similar seasonality in primary OC emissions with  
17 increased emissions during Northern Hemisphere summer due to the enhanced contribution of  
18 Northern Hemisphere biomass burning emissions from temperate and boreal forests to the  
19 total OC fluxes. Kaiser et al. (2012) found systematic model underestimation of smoke  
20 aerosol optical depth (AOD) observed by MODIS that can be as high as a factor of 3 on the  
21 global scale when emissions from bottom-up inventories like GFED are used. Petrenko et al.  
22 (2012) have demonstrated that such underestimate strongly varies by region.

23 Similar to OC results are obtained for CO, as seen in Fig. 3, where during the biomass  
24 burning season different quantities of CO are calculated depending on the inventory used. At  
25 Yonagunijima (Fig. 3a) CO concentration differences computed using the different  
26 inventories maximize in spring and models are underestimating measurements by 25%. Such  
27 differences between inventories are large at the East Trout Lake station in Canada, where in  
28 June and July model results differ by up to 150 ppb (a factor of 2.5). These results reflect the  
29 extremely high emissions in the GFEDv3-ECLIPSE and GFEDv3 inventories for this region  
30 that are not seen in the measurements (Fig. 3b). The assumption that all emissions occur near  
31 the surface leads to about 60% higher CO surface concentrations than when emissions are  
32 distributed vertically. At the areas where biomass burning occurs and downwind of them,

1 these emissions contribute between 10 and 75% to the total CO levels during the burning  
2 season.

3 Comparisons of O<sub>3</sub> simulations with surface measurements (Fig. 4) show noticeable  
4 difference between the simulation that neglects wildfire emissions (S4.0) and all other  
5 simulations, at stations like Mt. Kenya (Fig. 4f), La Quiaca observatory (Fig. 4g) and Hok  
6 Tsui (Fig. 4d), which are located in the vicinity or outflow of tropical biomass burning. These  
7 are areas where O<sub>3</sub> levels are the most sensitive to the different biomass burning emission  
8 scenarios. For instance, at La Quiana observatory (Fig. 4g), differences as high as 10 ppb of  
9 O<sub>3</sub> (i.e. ~25%) are computed for October when using the different emission scenarios. The  
10 FINN inventory results in the highest computed O<sub>3</sub> levels, while omitting biomass burning  
11 reduces O<sub>3</sub> levels by ~35%. However, very small sensitivity is seen between the scenarios  
12 with wildfire emissions for the other locations in Fig. 4. Thus, evaluating these inventories  
13 requires densifying air quality monitoring close to the major biomass burning sources in the  
14 tropics, which are virtually absent. Furthermore, we have calculated the ratio of the standard  
15 deviation to the mean of all model simulations to identify locations where biomass burning  
16 emission inventories produce the largest model divergence. In Fig. 5 these ratios are shown  
17 for OC and indicate that systematic observations over boreal regions, Alaska, South Asia and  
18 Indonesia can help constrain the used biomass burning emission inventories.

## 19 **4.2 Comparison with ozonesondes and satellite observations**

20 Because the impact of biomass burning is not restricted to the surface concentrations of  
21 pollutants but also extends in the free troposphere, we have also compared model results with  
22 ozonesondes as well as with O<sub>3</sub> and CO mid tropospheric columns as observed by  
23 Tropospheric Emission Spectrometer (TES) satellite instrument. In addition, simulated O<sub>3</sub>  
24 profiles have been compared with available ozonesondes data from WDCGG after  
25 interpolating into layers of 50 hPa from surface to the top of the atmosphere as described in  
26 detail by Myriokefalikakis et al. (2015 in preparation). Figure S6 in the supplement shows  
27 that there is no statistical difference in the performance of the different scenarios with regard  
28 to ozonesonde observations.

29 Similar results are obtained from the comparison of model results to the TES global survey  
30 data version 4 with focus on the relatively sensitive in the middle/lower free troposphere,  
31 using data from 7 TES pressure levels between 800 and 400 hPa. The TES products are

1 provided in 67 levels in vertical with a varying layer thickness (Beer et al., 2001). In order to  
2 compare TM4-ECPL model results with the TES observations, the methods presented in  
3 (Voulgarakis et al., 2011) have been used. Thus, the 3 – hourly model outputs are sampled at  
4 the times and locations of the TES measurements, then they are interpolate onto the 67 TES  
5 pressure levels in vertical, and finally the TES a priori profiles and averaging kernels are  
6 applied. The processed observational and model data are regridded to original  $3^{\circ}\times 2^{\circ}$  in  
7 longitude by latitude horizontal resolution in order to smooth – out gaps in the observations.  
8 More details are provided in Myriokefalitakis et al. (in preparation, 2015) where a detailed  
9 model evaluation is presented including comparison with satellite observations.

10 Point-by-point comparisons of the results for the different simulations performed for the  
11 present study against available TES observations for all model grids on daily mean basis are  
12 shown in Figures S7 in the supplement. No simulation and thus no emission database stands  
13 out for its performance in reproducing the observations.

### 14 **4.3 Tropospheric loads**

15 The global annual mean tropospheric loads for selected gases and aerosol components as  
16 computed for the base case scenario (S0.0) are shown in Fig. 6 for OC, CO, NO<sub>x</sub>, O<sub>3</sub>, OH,  
17 and isoprene. Fig. S3 (in the supplement) shows similar results for BC, SO<sub>4</sub><sup>2-</sup>, NO<sub>3</sub><sup>-</sup>, HNO<sub>3</sub>  
18 and NH<sub>4</sub><sup>+</sup>. Although changes in the wildfire emissions do not significantly impact the global  
19 tropospheric load of most pollutants as shown in Table 5, regionally significant differences  
20 are computed (e.g. for BC, the difference can reach a factor of 7, Fig. S4b) as will be further  
21 discussed. The choice of wildfire emission inventory impacts on the calculated tropospheric  
22 load of tracers. The most sensitive pollutants to wildfire emissions are found to be OC and  
23 BC, while O<sub>3</sub> shows small sensitivity.

#### 24 **4.3.1 Contribution of wildfires emissions on tropospheric loads.**

25 The contribution of wildfires to the tropospheric load of pollutants can be calculated by  
26 comparison of S0.0 (base case) with S4.0 that neglects the emissions. Wildfires increase the  
27 tropospheric loads of: OC by ~30%, BC by ~35%, CO by about 13% , NH<sub>4</sub><sup>+</sup> by 10%, HNO<sub>3</sub>  
28 by 8%, NO<sub>x</sub> by 5%, and SO<sub>4</sub><sup>2-</sup> and O<sub>3</sub> by 3% (Table 5).

29 Previous studies for CO with the NOAA GFDL GCTM have shown biomass burning to  
30 contribute from 15 to 30% to the total CO background (Galanter et al., 2000). This is in

1 agreement with the measurements by Crouse et al. (2009) in central Mexico which attributed  
2 21-31% of CO load to biomass burning emissions. This impact presents large temporal and  
3 spatial variability since it occurs during the burning season that lasts only a few months per  
4 year and is marked by tropical and boreal forest fires. Ziemke et al. (2009) modeling study  
5 with the Global Modeling Initiative (GMI) chemical transport model shows a global increase  
6 in CO between 21% and 53% due to biomass burning. The tropospheric O<sub>3</sub> load has been  
7 shown to correlate with that of CO during biomass burning events with a slope of O<sub>3</sub>/CO of  
8 about 1 (Honrath et al., 2004). However, other studies have shown only small changes in the  
9 tropospheric ozone on global scale (4-5% increase computed by Ziemke et al. (2009)), where  
10 regionally different impacts are computed, ranging for 10%-40% increase depending on  
11 region and season (Galanter et al., 2000). Aircraft observations in Boreal Canada showed no  
12 distinguishable within the smoke plume and in clean air (Parrington et al. (2013), while  
13 substantial O<sub>3</sub> enhancement has been measured in air masses downwind fire locations (Palmer  
14 et al., 2013).

15 The spatial variability of the annual mean impact of wildfire emissions on the tropospheric  
16 loads of OC, CO, NO<sub>x</sub>, O<sub>3</sub>, OH and isoprene is depicted in Fig. 7a-f and on BC, SO<sub>4</sub><sup>2-</sup>, NO<sub>3</sub><sup>-</sup>,  
17 HNO<sub>3</sub> and NH<sub>4</sub><sup>+</sup> in Fig. S5a-e (supplement). The most affected pollutants are OC (Fig. 7a)  
18 and BC (Fig. S5a) with computed local reduction due to the omission of wildfires by almost  
19 100%, in agreement with previous studies where a reduction of 50 % has been measured in  
20 Beijing (Duan et al., 2004), and up to 66% in Central Mexico (Crouse et al., 2009). Our  
21 results also show that annual mean local impacts on O<sub>3</sub> and CO, pollutants that have strong  
22 secondary sources, maximize at 20-30% in the tropics. As expected, the NO<sub>x</sub> tropospheric  
23 load is mostly affected by biomass burning both in the extra-tropics since fires contribute by  
24 50% to the NO<sub>x</sub> load at the outflow of boreal fires and in the tropical regions of south  
25 America, Africa and N. Australia where burning is significant (Fig. 7c) in agreement with  
26 previous studies that show up to 75% reduction near equatorial Africa (Galanter et al., 2000).  
27 As a consequence of the NO<sub>x</sub> and O<sub>3</sub> reductions when fire emissions are omitted, the  
28 computed hydroxyl radical (OH) load (Fig. 7e) is significantly reduced (5-10%) over the same  
29 regions; while larger percent reductions are computed at high northern latitudes where OH  
30 loads are generally very low due to the very weak photochemistry there.

### 1 **4.3.2 Impact of injection height**

2 The effect of height distribution of wildfire emissions on the computed tropospheric loads has  
3 been studied by comparing the simulations SX.0 with the respective simulations SX.1. Fig. 8  
4 presents such comparisons for BC. Both OC and BC are strongly affected by the injection  
5 height parameterization, since emitting aerosols above the boundary layer reduces aerosols  
6 available near the surface for loss via dry deposition. The largest differences are computed for  
7 the high latitudes over N. America and China where emission height distribution assumptions  
8 can result in differences of about 25% (Fig. 8). Previous studies conducted with the GEOS-  
9 Chem model over the south eastern Asia during 2001, show a decrease of 20-40% of BC  
10 surface concentrations when injected at height (Jian and Fu, 2014). In the same study it is  
11 shown that biomass burning injection height has much larger impact on BC than CO (50%-  
12 150% more BC calculated at 700hPa, than when emitted in the boundary layer). Differences  
13 are positive over source areas (since more is emitted near the surface in SX.1) and negative  
14 downwind (since less is transported away from source regions due to the increased deposition  
15 flux at the source regions). Additional comparisons are presented in the supplementary  
16 material (Fig. S6a-f). Assumptions in the biomass burning emissions injection height  
17 marginally affect CO and O<sub>3</sub>, with computed differences in the global annual mean  
18 tropospheric load smaller than 2.5%.

### 19 **4.3.3 Chemical feedbacks between biomass burning and vegetation** 20 **emissions**

21 It is interesting to examine the impact of wildfire emissions on isoprene tropospheric load.  
22 Isoprene is the single most important biogenic volatile organic compound (BVOC) emitted by  
23 vegetation (more than 50% of total annual BVOC emissions). The changes in OH described  
24 in section 4.3.1 (Fig. 7e), the main tropospheric oxidant that consumes isoprene, led to  
25 opposite in sign changes of isoprene (Fig. 7f). Such results indicate a strong chemical  
26 feedback between biomass burning and species emitted by vegetation.

27 This feedback is linking isoprene destruction and aerosol formation via the oxidants  
28 (hydroxyl-OH- and nitrate-NO<sub>3</sub>- radicals and ozone) that consume isoprene and produce  
29 semi-volatile organics but also via primary biomass burning aerosols that provide surface for  
30 organics to condense on. In the presence of fires, for the same isoprene emissions from  
31 vegetation (Fig. 7e) more nitrogen oxides (NO<sub>x</sub>) (Fig. 7c) are emitted leading to higher OH

1 radicals in the extended biomass burning region (up to 20% regionally) and slightly lower  
2 over northern hemisphere regions with intensive anthropogenic NO<sub>x</sub> emissions and their  
3 outflow. Thus, isoprene ambient levels are reduced with the highest reduction over and  
4 downwind tropical forested areas. Isoprene global tropospheric column is calculated to be  
5 lower by 15% in S0.0 than in S4.0 (fig. 7f). However, due to the NO<sub>x</sub>-dependence of the semi-  
6 volatile organic compounds formation from isoprene oxidation the total isoprene\_SOA  
7 concentrations change little (2%). This implies an overall 13% reduction in semi-volatile  
8 organic compounds formation yield from isoprene oxidation that comes to compensate for the  
9 increased isoprene oxidation. In addition, the primary organic aerosols (POA) emitted by  
10 biomass burning provide surface for partitioning of semi-volatile compounds, thus  
11 significantly increasing the partitioning of organic vapors to the aerosol phase that in turn also  
12 stimulate further partitioning to the aerosol phase. Thus, the isoprene-SOA partitioning to the  
13 aerosol phase increases by 16% in depletion of the gas phase isoprene-SOA precursors. This  
14 enhancement is consistent with, although much lower than derived from results by Kanakidou  
15 et al. (2000) on the enhancement of SOA formation from biogenic VOC due to partitioning on  
16 POA from pollution sources. That earlier study was using higher aerosol yields from BVOC  
17 than here and did not account for the later studied NO<sub>x</sub>-dependence of these yields; it also  
18 presented changes due to both combustion and fossil fuel POA. It has also shown that the use  
19 of different parameters in the two product yield representation of SOA formation from BVOC  
20 can lead to up to 70% of differences in the computed SOA tropospheric burden depending on  
21 atmospheric conditions. Tsigaridis et al. (2006) have evaluated the importance of the  
22 consideration of NO<sub>x</sub>-dependent SOA formation by calculating changes in the SOA burden  
23 and characteristics and found that in the current troposphere about 72% of the total SOA mass  
24 is formed under NO<sub>x</sub>-driven chemistry while in the past this fraction was lower (48%). Note  
25 however that large uncertainties and gaps in knowledge exist in the kinetics of isoprene-  
26 aerosol formation. Rollins et al. (2009) studying the NO<sub>3</sub> radical-driven chemistry of  
27 isoprene-SOA formation, have demonstrated the complexity of isoprene chemistry with  
28 respect to SOA formation with a drastic increase in aerosol yield when both double bonds of  
29 isoprene are oxidized, thus documenting the aerosol yield dependence on the level of  
30 oxidation of the precursors. Ervens et al. (2008) investigations have shown that isoprene  
31 aqueous phase chemistry is more efficient (about 40% aerosol yield) than gas phase chemistry  
32 (about 3% of aerosol yield) in forming SOA and depends on the water content in the

1 atmosphere and the pH. Carlton et al. (2009) review of laboratory measurements, field  
2 experiments and modeling studies concerning SOA formation from isoprene, documented  
3 differences in SOA yield parameterizations that most rely on a single set of chamber  
4 experiments, while aerosol yields are known to depend on various factors including the  
5 relative importance of NO<sub>x</sub> versus peroxide chemistry, temperature (that affects aerosol  
6 components volatility based on their enthalpy of vaporization) and pre-existing aerosol  
7 loading. They have calculated differences in SOA load induced by the NO<sub>x</sub> dependence  
8 parameterizations that are up to 30% of the total simulated OA over Eastern USA.

9 This feedback in the presence of biomass burning emissions increases by about 18% the  
10 global mean aerosol yield from isoprene emissions that is defined as the ratio of the  
11 tropospheric load of secondary organic aerosol from isoprene oxidation to the emissions of  
12 isoprene, while locally this difference can exceed 40%. Impacts on the tropospheric loads of  
13 the first generation gaseous products of isoprene are smaller, i.e. about 10%. The  
14 supplementary figure S11 shows the spatial distribution of the percent changes in the aerosol  
15 yield from isoprene emissions as computed comparing simulations S4.0 and S0.0. This figure  
16 points to the areas where the impact of biomass burning emissions (in percent) on the  
17 apparent SOA yield from isoprene is calculated by our model to be significant. These areas  
18 are the high latitude zone of North America and Asia, the tropical regions over land as well as  
19 the outflow from biomass burning regions. Note however that most isoprene\_SOA formation  
20 occurs over land.

21 Our results demonstrate the strong coupling between tropospheric chemistry, biomass burning  
22 and vegetation emitted species. They show that it is critical for the evaluation of the impact of  
23 these emissions on tropospheric chemistry to consistently account for BVOC emissions from  
24 vegetation and the co-location/co-occurrence of biomass burning emissions in the area. Co-  
25 location of vegetation and biomass burning emissions is linked to the model grid size since  
26 co-location area increases with lowering the horizontal resolution of the model. In this  
27 respect, to further investigate the impact of the feedback strength to the model resolution, a  
28 lower resolution set of simulations has been also performed. These low resolution simulations  
29 give results similar to the higher resolution with regard to the feedback strength (relative  
30 changes between S0.0 and S4.0). Thus, the percent increases do not seem to be affected by the  
31 resolution of the model, while the computed tropospheric loads of isoprene and secondary

1 organic aerosol differ between the high and low resolution simulations with low resolution  
2 simulation computing about 10% lower SOA and 4% lower isoprene loads.

### 3 **4.4 Tropospheric lifetimes**

4 The lifetimes of pollutants provide a measure of pollutant persistence in the atmosphere. They  
5 are here computed as the ratio of the tropospheric load to the loss rate (sum of chemical loss  
6 and deposition fluxes) for each model column (first 22 vertical layers of the model). Global  
7 mean tropospheric lifetimes are derived from the computed global burdens and losses.  
8 Changes in chemistry as discussed above, as well as changes in deposition of pollutants due to  
9 the modification of their spatial distribution, affect the lifetime of these compounds in the  
10 troposphere. Thus, isoprene's lifetime is increased in S4.0, as previously explained, by almost  
11 20% compared to S0.0. The global tropospheric lifetimes of all other species are less  
12 impacted by the choice of the emission inventory, with a maximum of about 12% for OC.  
13 This is in agreement with previously calculated differences reported in literature. For instance,  
14 such differences resulting from the use of 3 different biomass burning inventories (two global  
15 and one regional) in the TM4 model coupled with the CBM4 chemical mechanism do not  
16 exceed 5% for the African domain (Williams et al. (2012)). Table 6 shows the calculated  
17 global tropospheric lifetimes of pollutants for each scenario. The maximum percentage  
18 differences from the base case scenario (S0.0) are computed for the S4.0 simulation that  
19 neglects all wildfire emissions.

20 The lifetimes of pollutants, computed as the ratio of the tropospheric load to the loss rate (sum  
21 of chemical loss and deposition fluxes) for each model column, show sensitivity to both the  
22 height distribution of the emissions and the different emission inventories. The sensitivity of  
23 the BC lifetime to the height of injection of the biomass burning emissions is depicted in Fig.  
24 9, where the difference in calculated tropospheric lifetimes of OC attributed to emission  
25 injection height alone can reach 30% (right panels). The differences produced by injection  
26 height for other species are provided in Fig. S7 (supplement). The use of different biomass  
27 burning emission inventories led to up to almost 90% local differences for OC as seen in Fig.  
28 9g. The maximum differences are computed in the tropics and over the boreal forests in  
29 Canada and eastern Russia using the ACCMIP and FINN inventories (Fig. 9e,g). The overall  
30 impact of biomass burning emissions (simulations S4.0 versus S0.0) on the regional lifetimes  
31 of tracers is shown in Fig. 10, where significant increases in O<sub>3</sub> (up to about 25%) and CO (up



1 to about a factor of 2) lifetimes are calculated when wild fire emissions are neglected.  
2 Biomass burning is reducing O<sub>3</sub> lifetime in the burning regions of the tropics and the boreal  
3 forests. This is mainly due to the reaction of O<sub>3</sub> with NO emissions and subsequent HNO<sub>3</sub>  
4 formation. The impact of fire emissions on chemistry can be seen through the increases in the  
5 regional lifetime of CO and isoprene in S4.0 (Fig. 10a,d), where local differences can reach  
6 160%. OC and BC lifetimes are highly affected with local computed differences up to almost  
7 90% (OC) and 150% (BC) (Fig. 10e-f). Similar results are produced for SO<sub>4</sub><sup>2-</sup> lifetimes where  
8 the local differences in calculated tropospheric lifetimes range from about -25% to 25% near  
9 the tropics (Fig. 10g) and above the boreal forests of Russia and Canada where most open  
10 biomass burning events occur. Note that aerosols species like OC and BC have significant  
11 primary emissions from biomass burning and are removed from the atmosphere by dry and  
12 wet deposition, while carbon monoxide, isoprene and O<sub>3</sub> loads and lifetimes are driven by  
13 strong chemical production and loss terms. Thus, aerosol species behave differently than these  
14 short lived chemically reactive gases.

15 The tropospheric NO<sub>y</sub> lifetime (NO<sub>y</sub>=sum of NO<sub>x</sub>, HNO<sub>3</sub>, peroxyacetyl nitrate and organic  
16 nitrates) due to depositional losses strongly responds to the wild fire emissions used in the  
17 model, with differences between about -40% and 70% when taking into account all  
18 simulations that have been performed for this study. Focusing on central Canada and north  
19 eastern Asia, the S2.0 simulation results in a large increase in NO<sub>y</sub> lifetime compared to S0.0  
20 (Fig. 11b) that is weaker for the S1.0 (Fig. 11a). These differences are mainly attributed to the  
21 spatial distribution of the emissions favoring different chemistry pathways and resulting in  
22 different fractional composition of NO<sub>y</sub> and thus different dry and wet removal fluxes. Note  
23 that high differences in NO<sub>y</sub> lifetime due to deposition are calculated over the tropical regions  
24 with both positive and negative differences over and off-shore tropical Africa. There, both  
25 NO<sub>y</sub> burden and deposition losses are increasing due to biomass burning emissions and the  
26 corresponding NO<sub>y</sub> lifetime in S0.0 varies roughly between 4 to 50 days (Figure S12a). When  
27 wild fire emissions are omitted in the model, the absolute differences in NO<sub>y</sub> lifetime between  
28 simulations S4.0 and S0.0 in the tropics vary from -6.5 to +5 days (Figure S12b). Thus, the  
29 NO<sub>y</sub> lifetime is increased by up to 67% locally (Fig. 11d), although on global scale a small  
30 lifetime change (about -2%) is computed (Table 6).

## 1 **5 Conclusions**

2 The CTM sensitivity simulations performed here show that the choice of wildfire emission  
3 inventory has a significant impact on the simulated tropospheric concentrations of both  
4 primary emitted and secondary produced species, and as a result on the tropospheric lifetimes  
5 of gaseous and aerosol pollutants.

6 The differences introduced by the choice of biomass burning emissions are usually between -  
7 30% and 30% above and downwind of biomass burning hotspots (near the tropics, boreal  
8 forests of Russia and Canada) and can reach up to a factor of about 7 (e.g. for BC Fig. S4).  
9 These impacts maximize for primary pollutants over source areas and for secondary pollutants  
10 downwind. They are either due to the spatial and temporal differences in the emitted amounts  
11 of primary pollutants, or to the resulting changes in the levels of oxidants and thus to the  
12 impact of the primary pollutants on the concentrations of the chemically produced or  
13 destroyed tracers. The injection height of the wildfire emissions is found to affect both the  
14 tropospheric load and the lifetimes of the pollutants. Regionally up to 30% differences are  
15 computed in the calculated tropospheric lifetimes of pollutants. Tropospheric column of OC is  
16 mostly affected by different emission injection height with regional differences ranging from -  
17 20% to 25% and those attributed to the different emission inventories ranging from -70% to  
18 450% (Fig. S8b).

19 Interestingly, isoprene, mainly emitted by vegetation, shows sensitivity to the biomass  
20 burning emissions, with increasing tropospheric concentrations (and lifetime) when fire  
21 emissions decrease mainly due to the reduction in OH radical concentrations. This leads to an  
22 increase of the global mean aerosol yield from isoprene, defined as the ratio of tropospheric  
23 loads of secondary aerosol from isoprene oxidation to isoprene emissions, by about 18%  
24 when biomass burning emissions are taken into account. This fractional increase shows no  
25 sensitivity to the model resolution.

26 Finally, comparison of model results to observations shows the limitations of current  
27 observations in evaluating the biomass burning emission inventories. Such evaluation requires  
28 densifying air quality monitoring close to and downwind the major biomass burning sources  
29 in the tropics, as well as over boreal regions, Alaska, South Asia and Indonesia where our  
30 simulations using different biomass burning emission inventories show the larger diversity.

## 1 **6 Acknowledgements**

2 This work has been supported by the EU-FP7 project ECLIPSE (FP7-ENV-2011-282688).  
3 ND acknowledges support from the EU-FP7 project PEGASOS (FP7-ENV-2010-265148).  
4 The authors would like to thank the reviewers for their pertinent comments that helped  
5 improving this work.

## 6 **References**

- 7 Akagi, S. K., Yokelson, R. J., Wiedinmyer, C., Alvarado, M. J., Reid, J. S., Karl, T., Crouse,  
8 J. D., and Wennberg, P. O.: Emission factors for open and domestic biomass burning for use  
9 in atmospheric models, *Atmos. Chem. Phys.*, 11, 4039-4072, doi: 10.5194/acp-11-4039-2011,  
10 2011.
- 11 Andreae, M. O. and Merlet, P.: Emission of trace gases and aerosols from biomass burning,  
12 *Global Biogeochem. Cy.*, 15, 955-966, doi: 10.1029/2000GB001382, 2001.
- 13 Beer, R., Glavich, T. A., and Rider, D. M.: Tropospheric emission spectrometer for the Earth  
14 Observing System's Aura satellite, *Appl. Opt.*, 40, 2356-2367, doi: 10.1364/AO.40.002356,  
15 2001.
- 16 Bond, T. C., Streets, D. G., Yarber, K. F., Nelson, S. M., Woo, J.-H., and Klimont, Z.: A  
17 technology-based global inventory of black and organic carbon emissions from combustion, *J.*  
18 *Geophys. Res.-Atmos.*, 109, D14203, doi: 10.1029/2003JD003697, 2004.
- 19 Carlton, A. G., Wiedinmyer, C., and Kroll, J. H.: A review of Secondary Organic Aerosol  
20 (SOA) formation from isoprene, *Atmos. Chem. Phys.*, 9, 4987-5005, doi: 10.5194/acp-9-  
21 4987-2009, 2009.
- 22 Chatfield, R. B. and Delany, A. C.: Convection links biomass burning to increased tropical  
23 ozone: However, models will tend to overpredict O<sub>3</sub>, *J. Geophys. Res.-Atmos.*, 95, 18473-  
24 18488, doi: 10.1029/JD095iD11p18473, 1990.
- 25 Colarco, P. R., Schoeberl, M. R., Doddridge, B. G., Marufu, L. T., Torres, O., and Welton, E.  
26 J.: Transport of smoke from Canadian forest fires to the surface near Washington, D.C.:  
27 Injection height, entrainment, and optical properties, *J. Geophys. Res.-Atmos.*, 109, D06203,  
28 doi: 10.1029/2003JD004248, 2004.
- 29 Crouse, J. D., DeCarlo, P. F., Blake, D. R., Emmons, L. K., Campos, T. L., Apel, E. C.,  
30 Clarke, A. D., Weinheimer, A. J., McCabe, D. C., Yokelson, R. J., Jimenez, J. L., and  
31 Wennberg, P. O.: Biomass burning and urban air pollution over the Central Mexican Plateau,  
32 *Atmos. Chem. Phys.*, 9, 4929-4944, doi: 10.5194/acp-9-4929-2009, 2009.
- 33 Crutzen, P. J.: An overview of atmospheric chemistry. In: *Topics in Atmospheric and*  
34 *Interstellar Physics and Chemistry*, Boutron, C. F. (Ed.), Les Editions de Physique, France,  
35 1994.
- 36 Crutzen, P. J. and Andreae, M. O.: Biomass Burning in the Tropics: Impact on Atmospheric  
37 Chemistry and Biogeochemical Cycles, *Science*, 250, 1669-1678, doi:  
38 10.1126/science.250.4988.1669, 1990.
- 39 Dee, D. P., Uppala, S. M., Simmons, A. J., Berrisford, P., Poli, P., Kobayashi, S., Andrae, U.,  
40 Balmaseda, M. A., Balsamo, G., Bauer, P., Bechtold, P., Beljaars, A. C. M., van de Berg, L.,

- 1 Bidlot, J., Bormann, N., Delsol, C., Dragani, R., Fuentes, M., Geer, A. J., Haimberger, L.,  
2 Healy, S. B., Hersbach, H., Hólm, E. V., Isaksen, I., Kållberg, P., Köhler, M., Matricardi, M.,  
3 McNally, A. P., Monge-Sanz, B. M., Morcrette, J. J., Park, B. K., Peubey, C., de Rosnay, P.,  
4 Tavolato, C., Thépaut, J. N., and Vitart, F.: The ERA-Interim reanalysis: configuration and  
5 performance of the data assimilation system, *Q. J. Roy. Meteor. Soc.*, 137, 553-597, doi:  
6 10.1002/qj.828, 2011.
- 7 Dentener, F., Kinne, S., Bond, T., Boucher, O., Cofala, J., Generoso, S., Ginoux, P., Gong, S.,  
8 Hoelzemann, J. J., Ito, A., Marelli, L., Penner, J. E., Putaud, J. P., Textor, C., Schulz, M., van  
9 der Werf, G. R., and Wilson, J.: Emissions of primary aerosol and precursor gases in the years  
10 2000 and 1750 prescribed data-sets for AeroCom, *Atmos. Chem. Phys.*, 6, 4321-4344, doi:  
11 10.5194/acp-6-4321-2006, 2006.
- 12 Dirksen, R. J., Folkert Boersma, K., de Laat, J., Stammes, P., van der Werf, G. R., Val  
13 Martin, M., and Kelder, H. M.: An aerosol boomerang: Rapid around-the-world transport of  
14 smoke from the December 2006 Australian forest fires observed from space, *J. Geophys.*  
15 *Res.-Atmos.*, 114, D21201, doi: 10.1029/2009JD012360, 2009.
- 16 Duan, F., Liu, X., Yu, T., and Cachier, H.: Identification and estimate of biomass burning  
17 contribution to the urban aerosol organic carbon concentrations in Beijing, *Atmospheric*  
18 *Environment*, 38, 1275-1282, doi: 10.1016/j.atmosenv.2003.11.037, 2004.
- 19 Edwards, D. P., Emmons, L. K., Gille, J. C., Chu, A., Attié, J. L., Giglio, L., Wood, S. W.,  
20 Haywood, J., Deeter, M. N., Massie, S. T., Ziskin, D. C., and Drummond, J. R.: Satellite-  
21 observed pollution from Southern Hemisphere biomass burning, *J. Geophys. Res.-Atmos.*,  
22 111, D14312, doi: 10.1029/2005JD006655, 2006.
- 23 Ervens, B., Carlton, A. G., Turpin, B. J., Altieri, K. E., Kreidenweis, S. M., and Feingold, G.:  
24 Secondary organic aerosol yields from cloud-processing of isoprene oxidation products,  
25 *Geophysical Research Letters*, 35, L02816, doi: 10.1029/2007GL031828, 2008.
- 26 Field, R. D., van der Werf, G. R., and Shen, S. S. P.: Human amplification of drought-induced  
27 biomass burning in Indonesia since 1960, *Nature Geosci*, 2, 185-188, doi: 10.1038/ngeo443,  
28 2009.
- 29 Fountoukis, C. and Nenes, A.: ISORROPIA II: a computationally efficient thermodynamic  
30 equilibrium model for  $K^+$  -  $Ca^{2+}$  -  $Mg^{2+}$  -  $NH_4^+$  -  $Na^+$  -  $SO_4^{2-}$  -  $NO_3^-$  -  $Cl^-$  -  $H_2O$  aerosols, *Atmos.*  
31 *Chem. Phys.*, 7, 4639-4659, doi: 10.5194/acp-7-4639-2007, 2007.
- 32 Freitas, S. R., Longo, K. M., Chatfield, R., Latham, D., Silva Dias, M. A. F., Andreae, M. O.,  
33 Prins, E., Santos, J. C., Gielow, R., and Carvalho Jr, J. A.: Including the sub-grid scale plume  
34 rise of vegetation fires in low resolution atmospheric transport models, *Atmos. Chem. Phys.*,  
35 7, 3385-3398, doi: 10.5194/acp-7-3385-2007, 2007.
- 36 Fromm, M., Alfred, J., Hoppel, K., Hornstein, J., Bevilacqua, R., Shettle, E., Servranckx, R.,  
37 Li, Z., and Stocks, B.: Observations of boreal forest fire smoke in the stratosphere by POAM  
38 III, SAGE II, and lidar in 1998, *Geophys. Res. Lett.*, 27, 1407-1410, doi:  
39 10.1029/1999GL011200, 2000.
- 40 Galanter, M., Levy, H., and Carmichael, G. R.: Impacts of biomass burning on tropospheric  
41 CO, NO<sub>x</sub>, and O<sub>3</sub>, *J. Geophys. Res.-Atmos.*, 105, 6633-6653, doi: 10.1029/1999JD901113,  
42 2000.
- 43 Granier, C., Bessagnet, B., Bond, T., D'Angiola, A., Denier van der Gon, H., Frost, G., Heil,  
44 A., Kaiser, J., Kinne, S., Klimont, Z., Kloster, S., Lamarque, J.-F., Liousse, C., Masui, T.,

1 Meleux, F., Mieville, A., Ohara, T., Raut, J.-C., Riahi, K., Schultz, M., Smith, S., Thompson,  
2 A., van Aardenne, J., van der Werf, G., and van Vuuren, D.: Evolution of anthropogenic and  
3 biomass burning emissions of air pollutants at global and regional scales during the 1980–  
4 2010 period, *Climatic Change*, 109, 163-190, doi: 10.1007/s10584-011-0154-1, 2011.

5 Guan, H., Chatfield, R. B., Freitas, S. R., Bergstrom, R. W., and Longo, K. M.: Modeling the  
6 effect of plume-rise on the transport of carbon monoxide over Africa with NCAR CAM,  
7 *Atmos. Chem. Phys.*, 8, 6801-6812, doi: 10.5194/acp-8-6801-2008, 2008.

8 Guenther, A. B., Jiang, X., Heald, C. L., Sakulyanontvittaya, T., Duhl, T., Emmons, L. K.,  
9 and Wang, X.: The Model of Emissions of Gases and Aerosols from Nature version 2.1  
10 (MEGAN2.1): an extended and updated framework for modeling biogenic emissions, *Geosci.*  
11 *Model Dev.*, 5, 1471-1492, doi: 10.5194/gmd-5-1471-2012, 2012.

12 Hodzic, A., Vautard, R., Chepfer, H., Goloub, P., Menut, L., Chazette, P., Deuzé, J. L.,  
13 Apituley, A., and Couvert, P.: Evolution of aerosol optical thickness over Europe during the  
14 August 2003 heat wave as seen from CHIMERE model simulations and POLDER data,  
15 *Atmos. Chem. Phys.*, 6, 1853-1864, doi: 10.5194/acp-6-1853-2006, 2006.

16 Honrath, R. E., Owen, R. C., Martin, M. V., Reid, J. S., Lapina, K., Fialho, P., Dziobak, M.  
17 P., Kleissl, J., and Westphal, D. L.: Regional and hemispheric impacts of anthropogenic and  
18 biomass burning emissions on summertime CO and O<sub>3</sub> in the North Atlantic lower free  
19 troposphere, *J. Geophys. Res.-Atmos.*, 109, doi: 10.1029/2004jd005147, 2004.

20 Jaffe, D., Bertschi, I., Jaeglé, L., Novelli, P., Reid, J. S., Tanimoto, H., Vingarzan, R., and  
21 Westphal, D. L.: Long-range transport of Siberian biomass burning emissions and impact on  
22 surface ozone in western North America, *Geophys. Res. Lett.*, 31, L16106, doi:  
23 10.1029/2004GL020093, 2004.

24 Jaffe, D. A. and Wigder, N. L.: Ozone production from wildfires: A critical review, *Atmos.*  
25 *Environ.*, 51, 1-10, doi: 10.1016/j.atmosenv.2011.11.063, 2012.

26 Jian, Y. and Fu, T. M.: Injection heights of springtime biomass-burning plumes over  
27 peninsular Southeast Asia and their impacts on long-range pollutant transport, *Atmos. Chem.*  
28 *Phys.*, 14, 3977-3989, doi: 10.5194/acp-14-3977-2014, 2014.

29 Kaiser, J. W., Heil, A., Andreae, M. O., Benedetti, A., Chubarova, N., Jones, L., Morcrette, J.  
30 J., Razinger, M., Schultz, M. G., Suttie, M., and van der Werf, G. R.: Biomass burning  
31 emissions estimated with a global fire assimilation system based on observed fire radiative  
32 power, *Biogeosciences*, 9, 527-554, doi: 10.5194/bg-9-527-2012, 2012.

33 Kanakidou, M. and Crutzen, P. J.: The photochemical source of carbon monoxide:  
34 Importance, uncertainties and feedbacks, *Chemosphere - Global Change Science*, 1, 91-109,  
35 doi: 10.1016/S1465-9972(99)00022-7, 1999.

36 Kanakidou, M., Duce, R. A., Prospero, J. M., Baker, A. R., Benitez-Nelson, C., Dentener, F.  
37 J., Hunter, K. A., Liss, P. S., Mahowald, N., Okin, G. S., Sarin, M., Tsigaridis, K., Uematsu,  
38 M., Zamora, L. M., and Zhu, T.: Atmospheric fluxes of organic N and P to the global ocean,  
39 *Global Biogeochem. Cy.*, 26, GB3026, doi: 10.1029/2011GB004277, 2012.

40 Kanakidou, M., Tsigaridis, K., Dentener, F. J., and Crutzen, P. J.: Human-activity-enhanced  
41 formation of organic aerosols by biogenic hydrocarbon oxidation, *Journal of Geophysical*  
42 *Research: Atmospheres*, 105, 9243-9354, doi: 10.1029/1999JD901148, 2000.

- 1 Keywood, M., Kanakidou, M., Stohl, A., Dentener, F., Grassi, G., Meyer, C. P., Torseth, K.,  
2 Edwards, D., Thompson, A. M., Lohmann, U., and Burrows, J.: Fire in the Air: Biomass  
3 Burning Impacts in a Changing Climate, *Crit. Rev. Env. Sci. Tec.*, 43, 40-83, doi:  
4 10.1080/10643389.2011.604248, 2013.
- 5 Klimont, Z., Smith, S. J., and Cofala, J.: The last decade of global anthropogenic sulfur  
6 dioxide: 2000–2011 emissions, *Environ. Res. Lett.*, 8, 014003, doi: 10.1088/1748-  
7 9326/8/1/014003, 2013.
- 8 Lamarque, J. F., Shindell, D. T., Josse, B., Young, P. J., Cionni, I., Eyring, V., Bergmann, D.,  
9 Cameron-Smith, P., Collins, W. J., Doherty, R., Dalsoren, S., Faluvegi, G., Folberth, G.,  
10 Ghan, S. J., Horowitz, L. W., Lee, Y. H., MacKenzie, I. A., Nagashima, T., Naik, V.,  
11 Plummer, D., Righi, M., Rumbold, S. T., Schulz, M., Skeie, R. B., Stevenson, D. S., Strode,  
12 S., Sudo, K., Szopa, S., Voulgarakis, A., and Zeng, G.: The Atmospheric Chemistry and  
13 Climate Model Intercomparison Project (ACCMIP): overview and description of models,  
14 simulations and climate diagnostics, *Geosci. Model Dev.*, 6, 179-206, doi: 10.5194/gmd-6-  
15 179-2013, 2013.
- 16 Lavoué, D., Liousse, C., Cachier, H., Stocks, B. J., and Goldammer, J. G.: Modeling of  
17 carbonaceous particles emitted by boreal and temperate wildfires at northern latitudes, *J.*  
18 *Geophys. Res.-Atmos.*, 105, 26871-26890, doi: 10.1029/2000JD900180, 2000.
- 19 Lelieveld, J., van Aardenne, J., Fischer, H., de Reus, M., Williams, J., and Winkler, P.:  
20 Increasing Ozone over the Atlantic Ocean, *Science*, 304, 1483-1487, doi:  
21 10.1126/science.1096777, 2004.
- 22 Leung, F.-Y. T., Logan, J. A., Park, R., Hyer, E., Kasischke, E., Streets, D., and Yurganov,  
23 L.: Impacts of enhanced biomass burning in the boreal forests in 1998 on tropospheric  
24 chemistry and the sensitivity of model results to the injection height of emissions, *J. Geophys.*  
25 *Res.-Atmos.*, 112, D10313, doi: 10.1029/2006JD008132, 2007.
- 26 Levine, J. S., Cofer, W. R., Cahoon, D. R., and Winstead, E. L.: A DRIVER FOR GLOBAL  
27 CHANGE, *Environ. Sci. Technol.*, 29, 120A-125A, doi: 10.1021/es00003a746, 1995.
- 28 Mutch, R. W.: Fighting Fire with Prescribed Fire: A Return to Ecosystem Health, *J. Forest.*,  
29 92, 31-33, 1994.
- 30 Myriokefalitakis, S., Tsigaridis, K., Mihalopoulos, N., Sciare, J., Nenes, A., Kawamura, K.,  
31 Segers, A., and Kanakidou, M.: In-cloud oxalate formation in the global troposphere: a 3-D  
32 modeling study, *Atmos. Chem. Phys.*, 11, 5761-5782, doi: 10.5194/acp-11-5761-2011, 2011.
- 33 Myriokefalitakis, S., Vignati, E., Tsigaridis, K., Papadimas, C., Sciare, J., Mihalopoulos, N.,  
34 Facchini, M. C., Rinaldi, M., Dentener, F. J., Ceburnis, D., Hatzianastasiou, N., O'Dowd, C.  
35 D., van Weele, M., and Kanakidou, M.: Global Modeling of the Oceanic Source of Organic  
36 Aerosols, *Advances in Meteorology*, 2010, 1-16, doi: 10.1155/2010/939171, 2010.
- 37 Nenes, A., Pandis, S., and Pilinis, C.: ISORROPIA: A New Thermodynamic Equilibrium  
38 Model for Multiphase Multicomponent Inorganic Aerosols, *Aquatic Geochemistry*, 4, 123-  
39 152, doi: 10.1023/A:1009604003981, 1998.
- 40 Palmer, P. I., Parrington, M., Lee, J. D., Lewis, A. C., Rickard, A. R., Bernath, P. F., Duck, T.  
41 J., Waugh, D. L., Tarasick, D. W., Andrews, S., Aruffo, E., Bailey, L. J., Barrett, E.,  
42 Bauguitte, S. J. B., Curry, K. R., Di Carlo, P., Chisholm, L., Dan, L., Forster, G., Franklin, J.  
43 E., Gibson, M. D., Griffin, D., Helmig, D., Hopkins, J. R., Hopper, J. T., Jenkin, M. E.,  
44 Kindred, D., Kliever, J., Le Breton, M., Matthiesen, S., Maurice, M., Moller, S., Moore, D. P.,

1 Oram, D. E., O'Shea, S. J., Owen, R. C., Pagniello, C. M. L. S., Pawson, S., Percival, C. J.,  
2 Pierce, J. R., Punjabi, S., Purvis, R. M., Remedios, J. J., Rotermund, K. M., Sakamoto, K. M.,  
3 da Silva, A. M., Strawbridge, K. B., Strong, K., Taylor, J., Trigwell, R., Tereszchuk, K. A.,  
4 Walker, K. A., Weaver, D., Whaley, C., and Young, J. C.: Quantifying the impact of BOREal  
5 forest fires on Tropospheric oxidants over the Atlantic using Aircraft and Satellites  
6 (BORTAS) experiment: design, execution and science overview, *Atmos. Chem. Phys.*, 13,  
7 6239-6261, doi: 10.5194/acp-13-6239-2013, 2013.

8 Parrington, M., Palmer, P. I., Lewis, A. C., Lee, J. D., Rickard, A. R., Di Carlo, P., Taylor, J.  
9 W., Hopkins, J. R., Punjabi, S., Oram, D. E., Forster, G., Aruffo, E., Moller, S. J., Bauguitte,  
10 S. J. B., Allan, J. D., Coe, H., and Leigh, R. J.: Ozone photochemistry in boreal biomass  
11 burning plumes, *Atmos. Chem. Phys.*, 13, 7321-7341, doi: 10.5194/acp-13-7321-2013, 2013.

12 Petrenko, M., Kahn, R., Chin, M., Soja, A., Kucsera, T., and Harshvardhan: The use of  
13 satellite-measured aerosol optical depth to constrain biomass burning emissions source  
14 strength in the global model GOCART, *Journal of Geophysical Research: Atmospheres*, 117,  
15 D18212, doi: 10.1029/2012JD017870, 2012.

16 Pfister, G., Hess, P. G., Emmons, L. K., Lamarque, J. F., Wiedinmyer, C., Edwards, D. P.,  
17 Pétron, G., Gille, J. C., and Sachse, G. W.: Quantifying CO emissions from the 2004 Alaskan  
18 wildfires using MOPITT CO data, *Geophys. Res. Lett.*, 32, L11809, doi:  
19 10.1029/2005GL022995, 2005.

20 Praplan, A. P., Barmet, P., Dommen, J., and Baltensperger, U.: Cyclobutyl methyl ketone as a  
21 model compound for pinonic acid to elucidate oxidation mechanisms, *Atmos. Chem. Phys.*,  
22 12, 10749-10758, doi: 10.5194/acp-12-10749-2012, 2012.

23 Reid, J. S., Eck, T. F., Christopher, S. A., Koppmann, R., Dubovik, O., Eleuterio, D. P.,  
24 Holben, B. N., Reid, E. A., and Zhang, J.: A review of biomass burning emissions part III:  
25 intensive optical properties of biomass burning particles, *Atmos. Chem. Phys.*, 5, 827-849,  
26 doi: 10.5194/acp-5-827-2005, 2005.

27 Rollins, A. W., Kiendler-Scharr, A., Fry, J. L., Brauers, T., Brown, S. S., Dorn, H. P., Dubé,  
28 W. P., Fuchs, H., Mensah, A., Mentel, T. F., Rohrer, F., Tillmann, R., Wegener, R.,  
29 Wooldridge, P. J., and Cohen, R. C.: Isoprene oxidation by nitrate radical: alkyl nitrate and  
30 secondary organic aerosol yields, *Atmos. Chem. Phys.*, 9, 6685-6703, doi: 10.5194/acp-9-  
31 6685-2009, 2009.

32 Rosenfeld, D.: TRMM observed first direct evidence of smoke from forest fires inhibiting  
33 rainfall, *Geophys. Res. Lett.*, 26, 3105-3108, doi: 10.1029/1999GL006066, 1999.

34 Simmonds, P. G., Manning, A. J., Derwent, R. G., Ciais, P., Ramonet, M., Kazan, V., and  
35 Ryall, D.: A burning question. Can recent growth rate anomalies in the greenhouse gases be  
36 attributed to large-scale biomass burning events?, *Atmos. Environ.*, 39, 2513-2517, doi:  
37 10.1016/j.atmosenv.2005.02.018, 2005.

38 Sindelarova, K., Granier, C., Bouarar, I., Guenther, A., Tilmes, S., Stavrakou, T., Müller, J.  
39 F., Kuhn, U., Stefani, P., and Knorr, W.: Global data set of biogenic VOC emissions  
40 calculated by the MEGAN model over the last 30 years, *Atmos. Chem. Phys.*, 14, 9317-9341,  
41 doi: 10.5194/acp-14-9317-2014, 2014.

42 Sofiev, M., Ermakova, T., and Vankevich, R.: Evaluation of the smoke-injection height from  
43 wild-land fires using remote-sensing data, *Atmos. Chem. Phys.*, 12, 1995-2006, doi:  
44 10.5194/acp-12-1995-2012, 2012.

1 Sofiev, M., Vankevich, R., Ermakova, T., and Hakkarainen, J.: Global mapping of maximum  
2 emission heights and resulting vertical profiles of wildfire emissions, *Atmos. Chem. Phys.*,  
3 13, 7039-7052, doi: 10.5194/acp-13-7039-2013, 2013.

4 Tsigaridis, K., Daskalakis, N., Kanakidou, M., Adams, P. J., Artaxo, P., Bahadur, R.,  
5 Balkanski, Y., Bauer, S. E., Bellouin, N., Benedetti, A., Bergman, T., Berntsen, T. K.,  
6 Beukes, J. P., Bian, H., Carslaw, K. S., Chin, M., Curci, G., Diehl, T., Easter, R. C., Ghan, S.  
7 J., Gong, S. L., Hodzic, A., Hoyle, C. R., Iversen, T., Jathar, S., Jimenez, J. L., Kaiser, J. W.,  
8 Kirkevåg, A., Koch, D., Kokkola, H., Lee, Y. H., Lin, G., Liu, X., Luo, G., Ma, X., Mann, G.  
9 W., Mihalopoulos, N., Morcrette, J. J., Müller, J. F., Myhre, G., Myriokefalitakis, S., Ng, N.  
10 L., O'Donnell, D., Penner, J. E., Pozzoli, L., Pringle, K. J., Russell, L. M., Schulz, M., Sciare,  
11 J., Seland, Ø., Shindell, D. T., Sillman, S., Skeie, R. B., Spracklen, D., Stavrakou, T.,  
12 Steenrod, S. D., Takemura, T., Tiitta, P., Tilmes, S., Tost, H., van Noije, T., van Zyl, P. G.,  
13 von Salzen, K., Yu, F., Wang, Z., Wang, Z., Zaveri, R. A., Zhang, H., Zhang, K., Zhang, Q.,  
14 and Zhang, X.: The AeroCom evaluation and intercomparison of organic aerosol in global  
15 models, *Atmos. Chem. Phys.*, 14, 10845-10895, doi: 10.5194/acp-14-10845-2014, 2014.

16 Tsigaridis, K. and Kanakidou, M.: Global modelling of secondary organic aerosol in the  
17 troposphere: a sensitivity analysis, *Atmos. Chem. Phys.*, 3, 1849-1869, doi: 10.5194/acp-3-  
18 1849-2003, 2003.

19 Tsigaridis, K. and Kanakidou, M.: Secondary organic aerosol importance in the future  
20 atmosphere, *Atmos. Environ.*, 41, 4682-4692, doi: 10.1016/j.atmosenv.2007.03.045, 2007.

21 Tsigaridis, K., Krol, M., Dentener, F. J., Balkanski, Y., Lathière, J., Metzger, S.,  
22 Hauglustaine, D. A., and Kanakidou, M.: Change in global aerosol composition since  
23 preindustrial times, *Atmos. Chem. Phys.*, 6, 5143-5162, doi: 10.5194/acp-6-5143-2006, 2006.

24 Val Martin, M., Kahn, R. A., Logan, J. A., Paugam, R., Wooster, M., and Ichoku, C.: Space-  
25 based observational constraints for 1-D fire smoke plume-rise models, *J. Geophys. Res.-*  
26 *Atmos.*, 117, n/a-n/a, doi: 10.1029/2012jd018370, 2012.

27 Val Martin, M., Logan, J. A., Kahn, R. A., Leung, F. Y., Nelson, D. L., and Diner, D. J.:  
28 Smoke injection heights from fires in North America: analysis of 5 years of satellite  
29 observations, *Atmos. Chem. Phys.*, 10, 1491-1510, doi: 10.5194/acp-10-1491-2010, 2010.

30 van der Werf, G. R., Randerson, J. T., Giglio, L., Collatz, G. J., Kasibhatla, P. S., and  
31 Arellano Jr, A. F.: Interannual variability in global biomass burning emissions from 1997 to  
32 2004, *Atmos. Chem. Phys.*, 6, 3423-3441, doi: 10.5194/acp-6-3423-2006, 2006.

33 van der Werf, G. R., Randerson, J. T., Giglio, L., Collatz, G. J., Mu, M., Kasibhatla, P. S.,  
34 Morton, D. C., DeFries, R. S., Jin, Y., and van Leeuwen, T. T.: Global fire emissions and the  
35 contribution of deforestation, savanna, forest, agricultural, and peat fires (1997–2009), *Atmos.*  
36 *Chem. Phys.*, 10, 11707-11735, doi: 10.5194/acp-10-11707-2010, 2010.

37 Vignati, E., Facchini, M. C., Rinaldi, M., Scannell, C., Ceburnis, D., Sciare, J., Kanakidou,  
38 M., Myriokefalitakis, S., Dentener, F., and O'Dowd, C. D.: Global scale emission and  
39 distribution of sea-spray aerosol: Sea-salt and organic enrichment, *Atmos. Environ.*, 44,  
40 670-677, doi: 10.1016/j.atmosenv.2009.11.013, 2010.

41 Voulgarakis, A., Telford, P. J., Aghedo, A. M., Braesicke, P., Faluvegi, G., Abraham, N. L.,  
42 Bowman, K. W., Pyle, J. A., and Shindell, D. T.: Global multi-year O<sub>3</sub>-CO correlation  
43 patterns from models and TES satellite observations, *Atmos. Chem. Phys.*, 11, 5819-5838,  
44 doi: 10.5194/acp-11-5819-2011, 2011.



1 Wiedinmyer, C., Akagi, S. K., Yokelson, R. J., Emmons, L. K., Al-Saadi, J. A., Orlando, J. J.,  
2 and Soja, A. J.: The Fire INventory from NCAR (FINN): a high resolution global model to  
3 estimate the emissions from open burning, *Geosci. Model Dev.*, 4, 625-641, doi:  
4 10.5194/gmd-4-625-2011, 2011.

5 Williams, J. E., Weele, M. v., Velthoven, P. F. J. v., Scheele, M. P., Liousse, C., and Werf, G.  
6 R. v. d.: The Impact of Uncertainties in African Biomass Burning Emission Estimates on  
7 Modeling Global Air Quality, Long Range Transport and Tropospheric Chemical Lifetimes,  
8 *Atmosphere*, 3, 132-163, doi: 10.3390/atmos3010132, 2012.

9 Ziemke, J. R., Chandra, S., Duncan, B. N., Schoeberl, M. R., Torres, O., Damon, M. R., and  
10 Bhartia, P. K.: Recent biomass burning in the tropics and related changes in tropospheric  
11 ozone, *Geophysical Research Letters*, 36, L15819, doi: 10.1029/2009GL039303, 2009.

12

13

1 **Table 1** Anthropogenic emissions (Tg a<sup>-1</sup>) used in this study and fraction of emissions that corresponds to the  
 2 AWB sector included in the ECLIPSE anthropogenic emissions inventory. Both absolute quantities and  
 3 percentage of the total anthropogenic emissions from (Klimont et al., 2013) are presented.

	<b>BC</b>	<b>CO</b>	<b>NO<sub>x</sub></b>	<b>OC</b>	<b>SO<sub>x</sub></b>	<b>NMVOC</b>
<b>ECLIPSE (with AWB)</b>	5.38	527.1	43.97	11.56	45.95	140.47
<b>AWB on ECLIPSE</b>	0.333	27.46	0.296	1.281	0.173	4.255
<b>% contribution of AWB to total anthropogenic</b>	6.19	5.21	0.67	11.08	0.38	3.03

4

5 **Table 2** Total annual amounts of pollutants emitted by wild fires according to the different inventories used, for  
 6 2008 in Tg a<sup>-1</sup>. NO<sub>x</sub> is reported as NO. (\*)GFEDv3.1 without the AWB is here called GFEDv3.1-ECLIPSE

	<b>BC</b>	<b>CO</b>	<b>NO<sub>x</sub></b>	<b>OC</b>	<b>SO<sub>2</sub></b>	<b>NMVOC</b>	<b>NH<sub>3</sub></b>	<b>Spatial resolution</b>	<b>Temporal resolution</b>
<b>GFEDv3.1-ECLIPSE*</b>	1.695	264.205	3.751	15.197	0.940	44.414.	3.320	0.5°x0.5°	Monthly
<b>FINN</b>	1.939	338.576	5.998	20.202	1.102	63.476	5.410	1°x1°	Monthly
<b>ACCMIP</b>	2.620	460.419	5.479	23.309	1.929	80.869	9.203	0.5°x0.5°	Monthly

7

8 **Table 3** Agricultural Waste Burning sector as provided for different emission inventories in Tg a<sup>-1</sup> for the year  
 9 2008. NO<sub>x</sub> is reported as NO

	<b>BC</b>	<b>CO</b>	<b>NO<sub>x</sub></b>	<b>OC</b>	<b>SO<sub>x</sub></b>	<b>NMVOC</b>
<b>ECLIPSE</b>	0.333	27.46	0.296	1.281	0.173	4.255
<b>GFEDv3.1</b>	0.064	12.57	0.143	0.497	0.027	1.296
<b>ACCMIP</b>	0.162	21.22	0.444	0.775	0.220	2.857

10

11

12 **Table 4** Summary of simulations performed for this work.

<b>Height</b>	<b>inventory</b>	<b>Varying</b>	<b>Surface</b>	<b>AWB</b>
<b>S0.0</b> <b>S0.1</b>	<b>GFEDv3 ECLIPSE</b>	<b>X</b>	<b>X</b>	<b>ECLIPSE</b>
<b>S1.0</b> <b>S1.1</b>	<b>GFEDv3.1</b>	<b>X</b>	<b>X</b>	<b>GFEDv3.1</b>
<b>S2.0</b> <b>S2.1</b>	<b>ACCMIP</b>	<b>X</b>	<b>X</b>	<b>ECLIPSE</b>
<b>S3.0</b> <b>S3.1</b>	<b>FINN</b>	<b>X</b>	<b>X</b>	<b>ECLIPSE</b>
<b>S4.0</b>	<b>zero</b>			<b>ECLIPSE</b>

13

14

1 **Table 5** Total annual mean tropospheric load of pollutants for all simulations in Tg a<sup>-1</sup>.

	<b>S0.0</b>	<b>S0.1</b>	<b>S1.0</b>	<b>S1.1</b>	<b>S2.0</b>	<b>S2.1</b>	<b>S3.0</b>	<b>S3.1</b>	<b>S4.0</b>
<b>CO</b>	319.12	318.37	317.26	316.20	341.47	339.63	331.58	330.37	283.88
<b>O<sub>3</sub></b>	416.17	415.52	415.35	414.82	422.17	421.29	423.04	422.03	405.25
<b>NO<sub>x</sub></b>	1.299	1.293	1.286	1.282	1.330	1.323	1.390	1.378	1.200
<b>SO<sub>4</sub><sup>2-</sup></b>	1.914	1.908	1.913	1.906	1.933	1.923	1.911	1.905	1.868
<b>HNO<sub>3</sub></b>	2.196	2.188	2.181	2.181	2.235	2.228	2.229	2.219	2.048
<b>NH<sub>4</sub><sup>+</sup></b>	0.498	0.487	0.514	0.496	0.516	0.496	0.507	0.492	0.460
<b>Isoprene</b>	0.266	0.267	0.267	0.268	0.247	0.248	0.253	0.254	0.315
<b>OC</b>	0.111	0.110	0.110	0.109	0.121	0.120	0.117	0.116	0.072
<b>BC</b>	0.136	0.135	0.131	0.131	0.146	0.146	0.133	0.133	0.088

2  
3  
4  
5

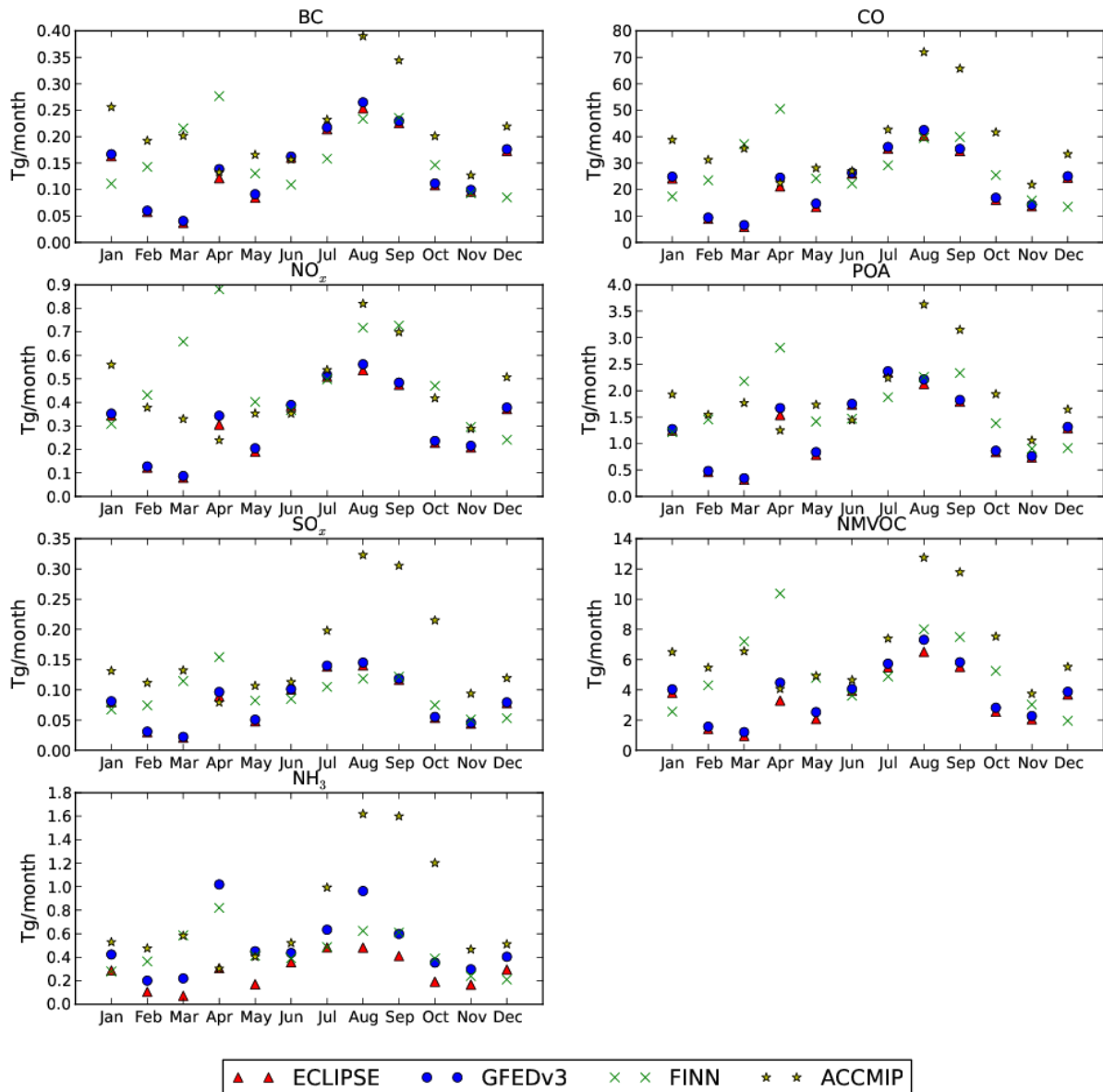
1 **Table 6** Calculated annual mean tropospheric lifetimes of pollutants for all the simulations performed.

	<b>S0.0</b>	<b>S0.1</b>	<b>S1.0</b>	<b>S1.1</b>	<b>S2.0</b>	<b>S2.1</b>	<b>S3.0</b>	<b>S3.1</b>	<b>S4.0</b>
<b>CO (days)</b>	41.48	41.44	41.43	41.35	41.82	41.67	41.45	41.40	41.67
<b>O<sub>3</sub> (days)</b>	24.58	24.62	24.59	24.63	24.39	24.43	24.33	24.39	25.19
<b>NO<sub>y</sub> (days)</b>	7.342	7.300	7.293	7.255	7.358	7.297	7.628	7.541	7.184
<b>SO<sub>4</sub><sup>2-</sup> (days)</b>	4.446	4.442	4.448	4.444	4.427	4.423	4.421	4.419	4.426
<b>HNO<sub>3</sub> (days)</b>	2.804	2.805	2.793	2.800	2.792	2.796	2.774	2.775	2.776
<b>NH<sub>4</sub><sup>+</sup> (days)</b>	4.979	4.932	5.032	4.962	4.961	4.905	4.928	4.894	4.862
<b>Isoprene (hours)</b>	4.457	4.475	4.466	4.482	4.137	4.152	4.236	4.250	5.270
<b>OC (days)</b>	6.031	5.998	6.046	6.012	5.925	5.894	5.839	5.819	5.302
<b>BC (days)</b>	6.927	6.908	6.962	6.941	6.889	6.871	6.583	6.572	6.261

2

3

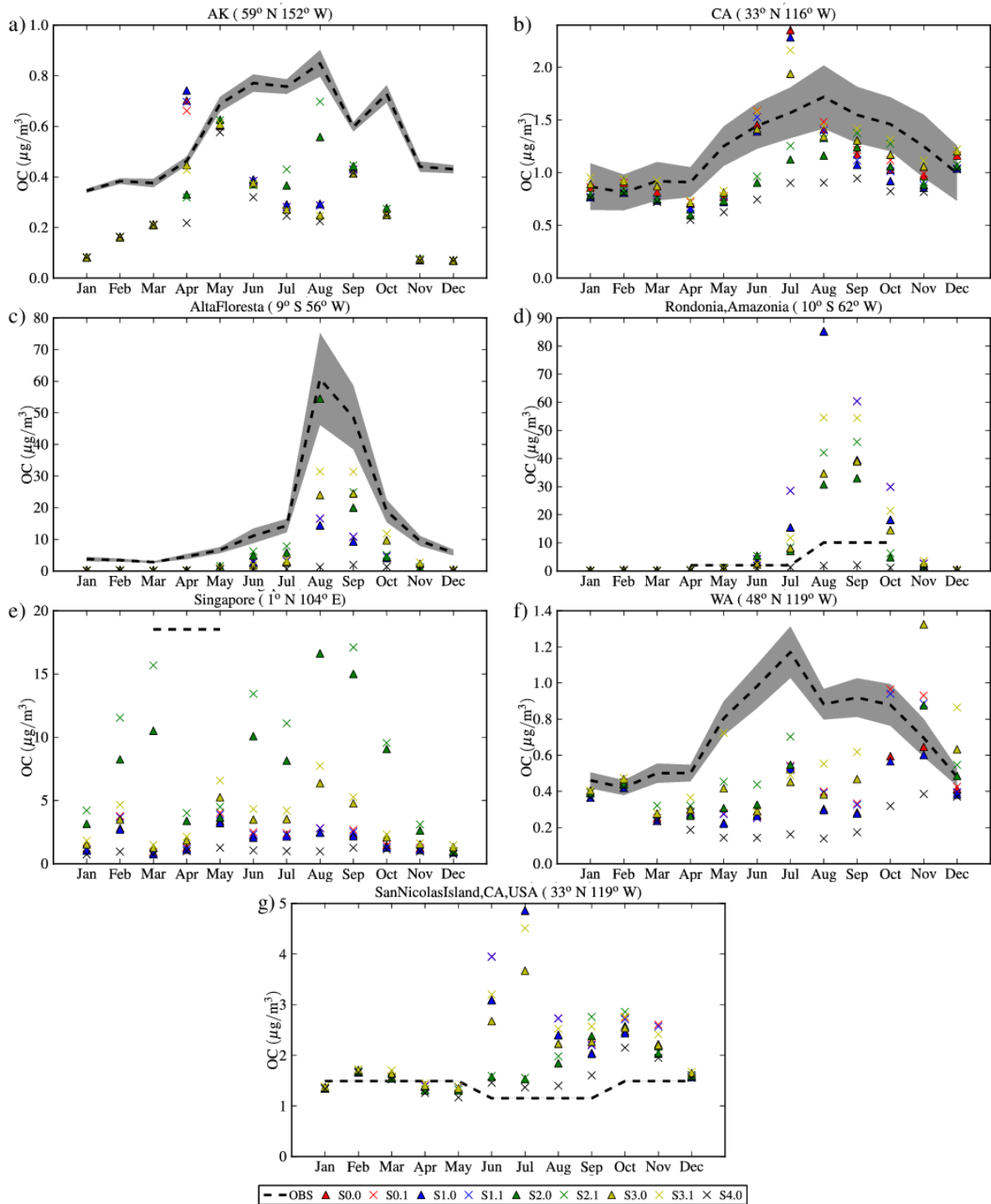
4



1

2 **Fig. 1** Monthly variation and differences of biomass burning emission inventories for the year 2008 for all  
 3 species used in the model. For simplicity, NMVOC are summed up. NO<sub>x</sub> are presented in NO, SO<sub>x</sub> in SO<sub>2</sub> and  
 4 NMVOCs in total mass.

5

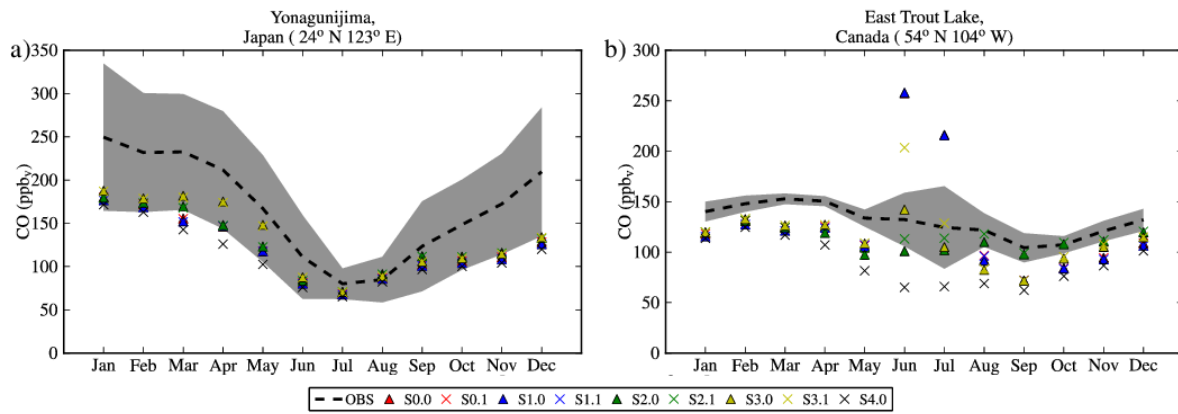


1

2 **Fig. 2** Comparison of monthly mean model results with observations of organic carbon (OC) at southern Alaska  
 3 (a), California State, USA (b), Alta Floresta, Brazil (c), Rondonia, Amazonia (d), Singapore (e), Washington  
 4 State, USA (f) and San Nicolas Island, California, USA (g). The dashed line with the gray shaded area shows the  
 5 monthly mean value of observations with the standard deviation based on their interannual variability, while the  
 6 colored symbols show the calculated values for the specific station. Triangles are for simulations assuming a  
 7 vertical distribution of wildfire emissions, while the x symbols show the simulations assuming that all open  
 8 biomass burning emissions occur near the surface. Details on the simulations are given in Table 4.

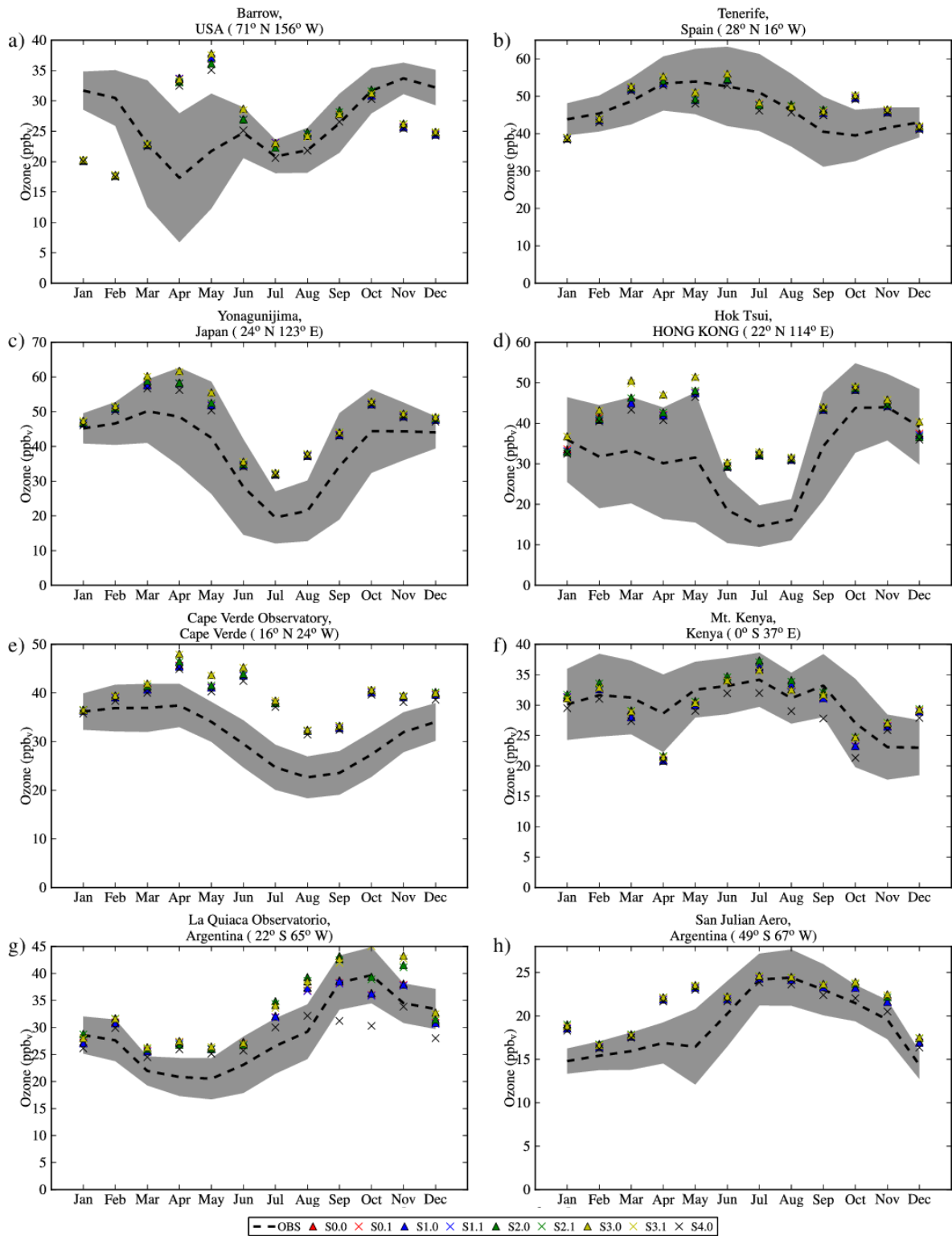
9

1



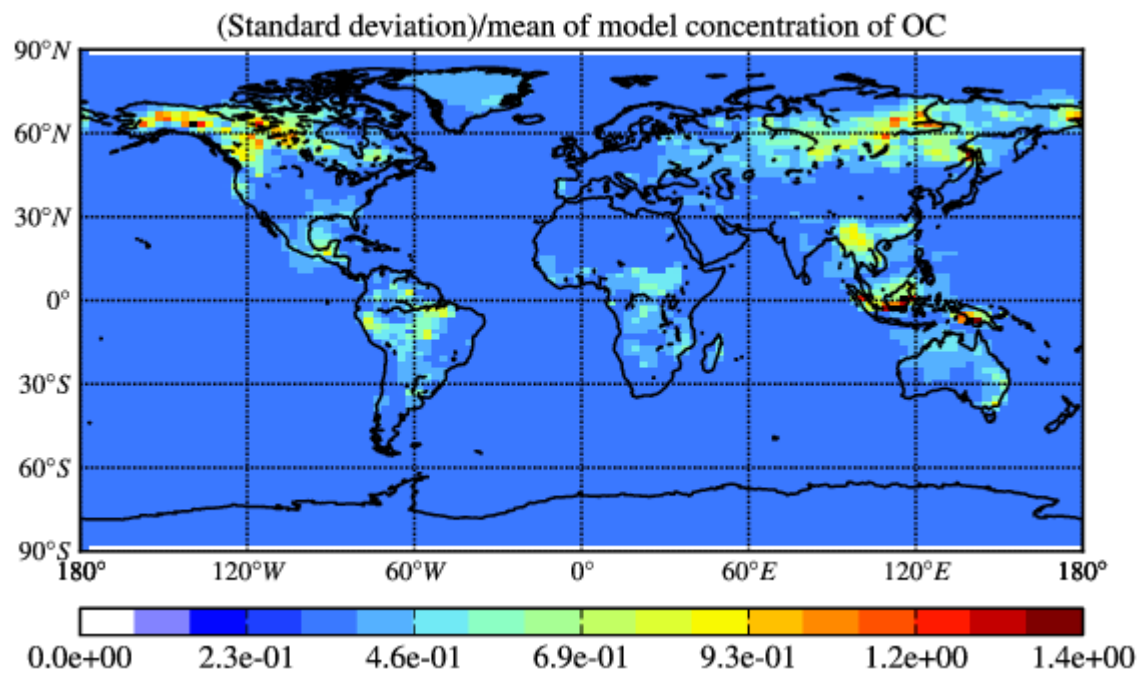
2

3 **Fig. 3** Comparison of monthly mean model results with CO surface observations at Yonagunijima, Japan (a) and  
4 at East Trout Lake, Canada (b). Lines and symbols as in Fig. 2 but for CO.

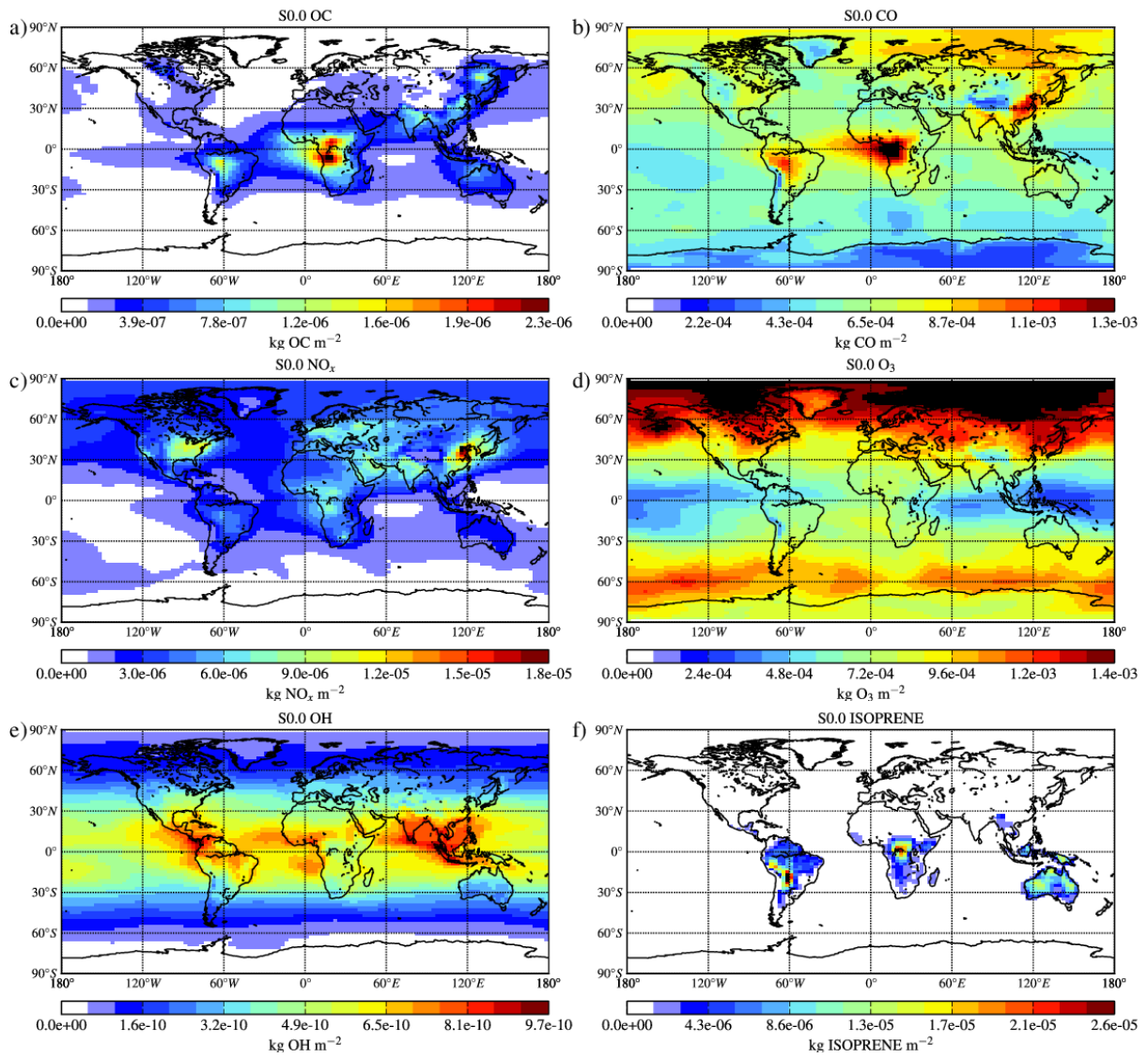


1  
 2 **Fig. 4** Comparison of monthly mean surface ozone measurements with model results at Barrow, USA (a),  
 3 Tenerife, Spain (b), Yonagunijima, Japan (c), Hok Tsui, Hong Kong (d), Cape Verde Observatory, Cape Verde  
 4 (e), Mount Kenya, Kenya (f), La Quiaca Observatory, Argentina (g) and San Julian Aero, Argentina (h) . Lines  
 5 and symbols as in Fig. 2 but for O<sub>3</sub>.

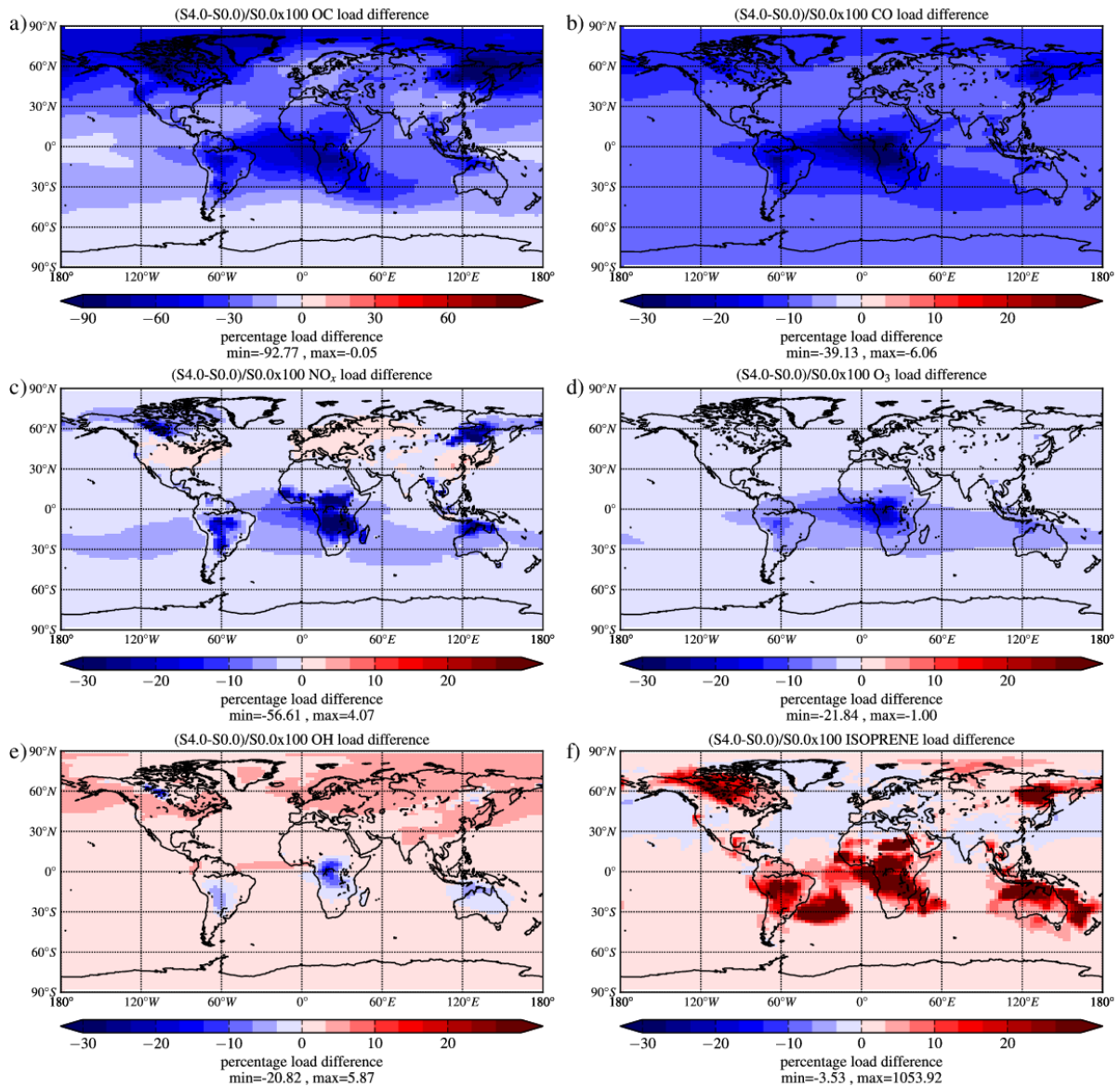




1  
 2 **Fig. 5** Spatial distribution of the ratio of the standard deviation to the mean of all model simulations, based on  
 3 annual mean of the computed surface OC concentrations.

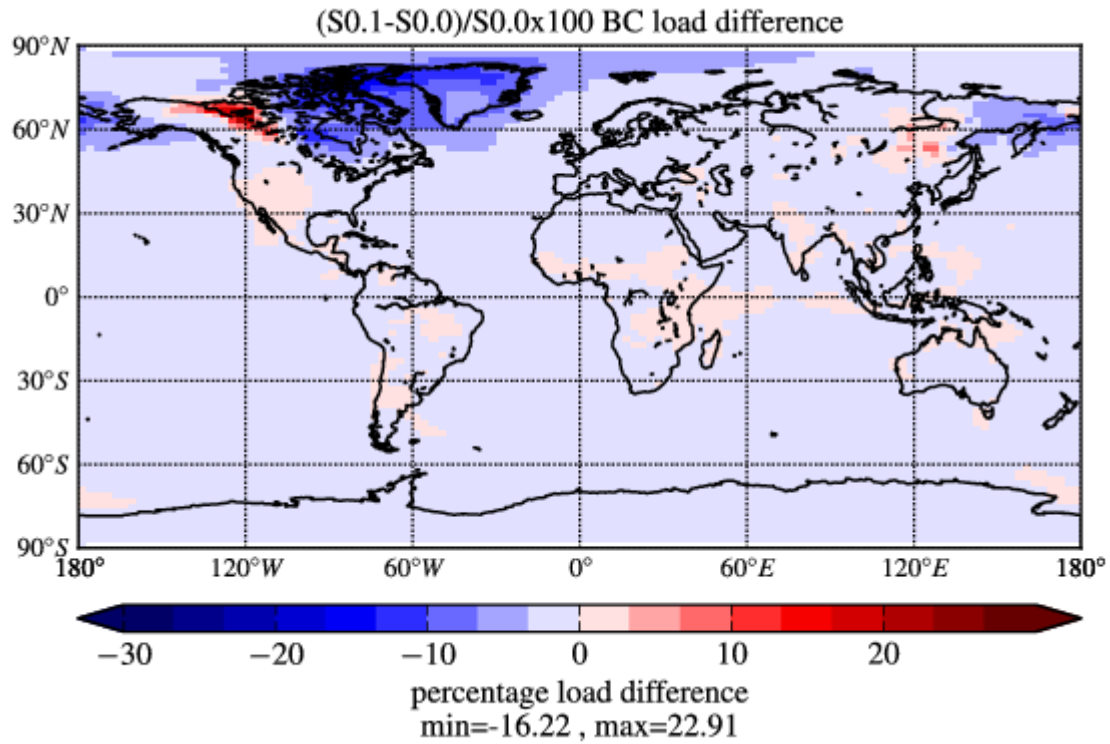


1  
 2 **Fig. 6** Calculated annual mean tropospheric load in ( $\text{Kg m}^{-2}$ ) of selected species for the base case scenario (S0.0).  
 3 Areas with black exceed the maximum value of the colorbar.  
 4



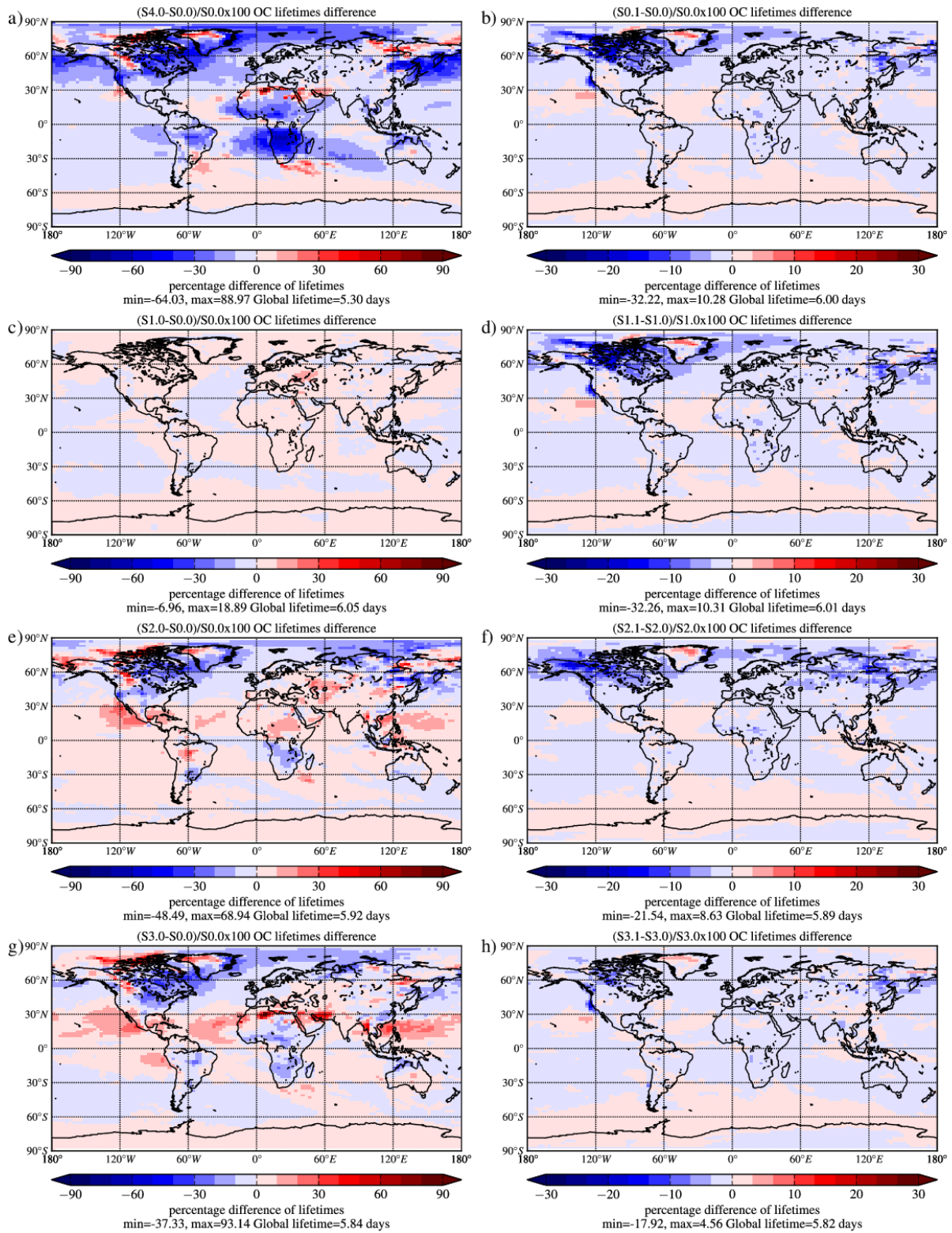
1  
2  
3  
4  
5  
6

**Fig. 7** Percentage difference in the computed annual mean tropospheric loads of OC (a), CO (b), NO<sub>x</sub> (c), O<sub>3</sub> (d), OH (e), isoprene (f) – attributed to wildfire emissions calculated as  $(\text{column}_{S4.0} - \text{column}_{S0.0})/(\text{column}_{S0.0}) \times 100$ . The scale is from -30% to 30% (-90% to 90% for OC); the minimum and maximum differences are printed under each panel.

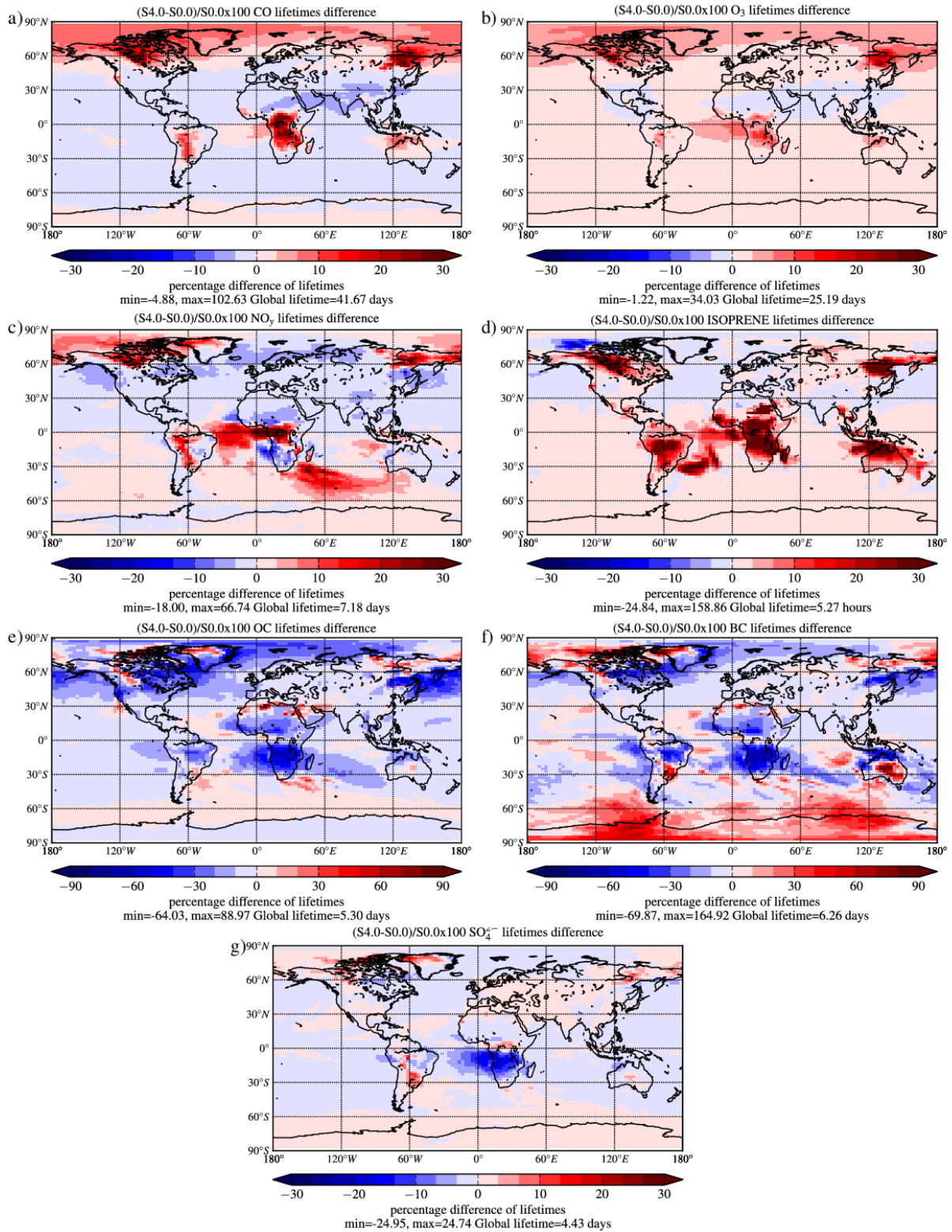


1  
2  
3  
4  
5

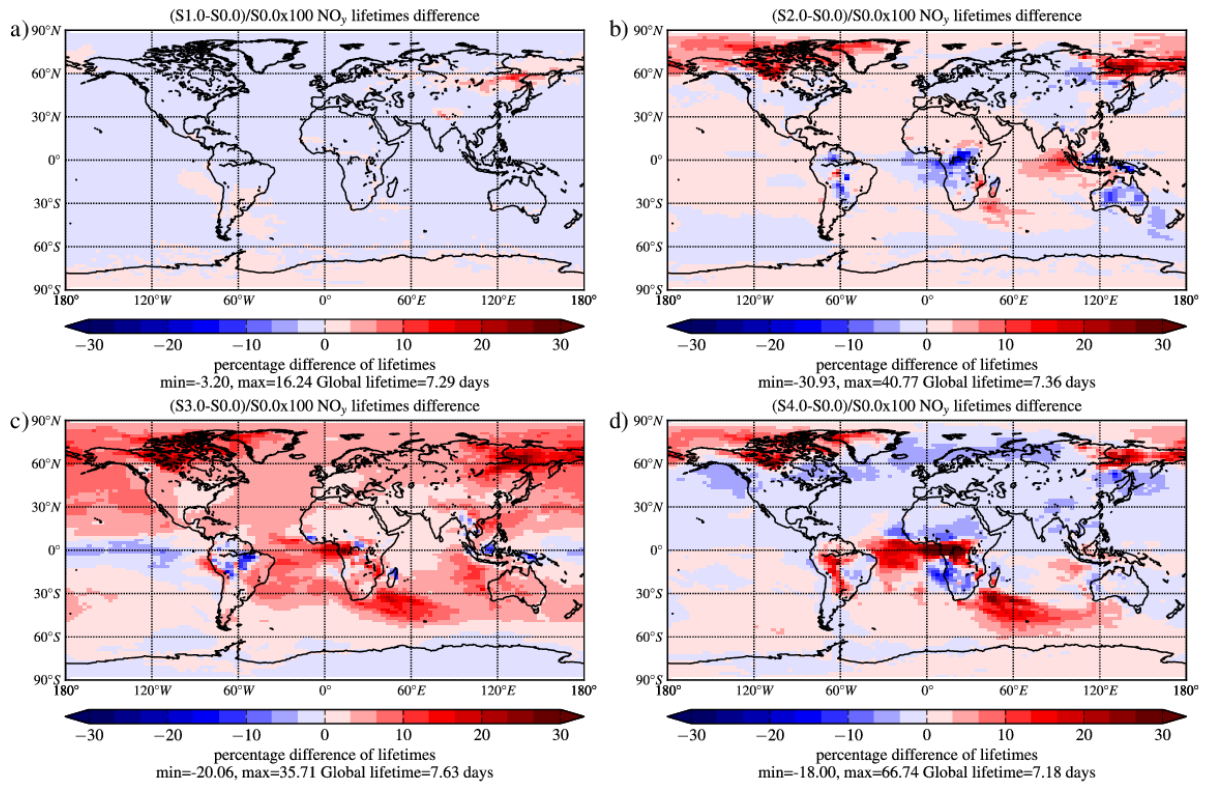
**Fig. 8** Percentage difference of annual mean computed tropospheric load of BC attributed to wildfire emission injection height calculated as  $(\text{load}_{S0.1} - \text{load}_{S0.0})/(\text{load}_{S0.0}) \times 100$ . The scale is from -30% to 30% ; the minimum and maximum percent differences are printed under each panel.



1  
2 **Fig. 9.** Percent impact on the computed annual mean tropospheric lifetime of OC of: (left panels) the different  
3 emission inventories calculated as the percent difference between simulations SX.0 and simulation S0.0; and of  
4 (right panels) height distribution calculated as the percent difference between simulations SX.1 and simulations  
5 SX.0.. The colorbar ranges from -90% to 90% for the surface differences and -30% to 30% for the differences  
6 induced by height distribution. The minimum and maximum local lifetimes percent changes as well as the global  
7 lifetime are printed under each panel.  
8



1  
 2 **Fig. 10** Percent impact of wild fire emissions to the computed annual mean tropospheric lifetimes of CO (a), O<sub>3</sub>  
 3 (b), NO<sub>y</sub> (c), isoprene (d), OC (e), BC (f) and SO<sub>4</sub><sup>2-</sup> (g) depicted as the percentage difference of S4.0 and S0.0.  
 4 The colorbar ranges from -30% to 30% (-90% to 90% for OC and BC). The minimum and maximum local  
 5 lifetimes percent changes as well as the global lifetime are printed under each panel.



1  
2  
3  
4  
5  
6  
7

**Fig. 11** Computed annual mean tropospheric NO<sub>y</sub> lifetimes differences between the base case scenario (S0.0) and S1.0 (a), S2.0 (b), S3.0 (c) and S4.0 (d), computed by reference to S0.0. The colorbar ranges from -30% to 30%. The minimum and maximum local lifetimes percent changes as well as the global lifetime are printed under each panel.